NASA Contractor Report 179426

Investigation of Empennage Buffeting

C. Edward Lan and I. G. Lee
Flight Research Laboratory
The University of Kansas Center for Research, Inc.
Lawrence, Kansas 66045

Appendix by
William H. Wentz, Jr.
Wichita State University

Prepared for
Ames Research Center
Dryden Flight Research Facility
Edwards, California
Under Contract NAG2-371
1987

National Aeronautics and
Space Administration
Ames Research Center
Dryden Flight Research Facility
Edwards, California 93523-5000

TABLE OF CONTENTS

LIST OF SYMBOLS

$A_{nj} = \iint \Delta C_{p_j} \phi_n \, d\bar{\xi} d\bar{\eta}$	the generalized aerodynamic force matrix
$BM_{E_n}(i\omega)$	bending moment transfer function due to externally applied load
$BM_{M_n}(i\omega)$	bending moment transfer function due to structural motion
b	span
b_o	reference length, e.g. the root semichord
c	local chord
$\bar{c}$	mean geometric chord
$\tilde{c}$	a characteristic length for augmented vortex lift
C_B	dimensionless buffeting coefficient
ΔC_{pj}	lifting pressure coefficient at point (x,y) on the wing caused by the motion of the j^{th} normal mode
$C_{BB}(M,\alpha)$	wing root strain signal/q_∞
$\overline{C}_{Bd}$	RMS values of root bending moment coefficient
c_S	sectional suction coefficient
$\bar{c}_S$	$= c_S \, c/\bar{c} \, \sin^2\alpha$
E^2	non-dimensional aerodynamic excitation parameter
$F(t)$	random forcing function
$\overline{F(t)^2}$	mean square value of F(t)
f	wing bending frequency, cps
g_n	structural damping coefficient for the n^{th} mode
$H_{BM}(\omega)$	bending moment transfer function

K	aerodynamic damping parameter
K_B	scaling factor
k	reduced frequency parameter
$\ell_E(y,t)$	sectional lift due to external forces
$\ell_M(y,t)$	sectional lift due to structural motion
$\bar{\ell}_{En}(y,i\omega)$	sectional lift due to a unit generalized force in the n^{th} mode
$\ell_s(\eta)$	length of the separated flow at a spanwise station of the wing
$M_o(t)$	root bending moment
$\overline{M_o^2}$	mean square values of root bending moment
$M_n = \iint \phi_n^2 \, m \, dx \, dy$	the generalized mass
$m(x,y)$	mass per unit area
n	frequency parameter
p_E	pressure loading due to externally applied disturbance
p_M	pressure loading due to structural motion
Δp_j	lifting pressure at point (x,y) on the wing caused by motion of the j^{th} normal mode
$\overline{p^2}$	total RMS pressure fluctuation
Q_n	the generalized force
$Q_n^E(t)$	random excitation force due to externally applied force
$q_n(t)$	generalized coordinates
$\dot{q}_n$	generalized velocity
$\ddot{q}_n$	generalized acceleration
$\overline{q_n}^2$	mean square displacement
$\overline{\ddot{q}_n}^2$	mean square acceleration

$q_\infty = \frac{1}{2} \rho V_\infty^2$	free stream dynamic pressure
r_1, r_2	$= (x_1, y_1), (x_2, y_2)$
$R_{12}(r_1, r_2, \tau)$	space-time correlation
$R_{b/s}$	ratio of buffeting vortex strength to steady vortex strength
$\bar{r}_{av} = \frac{1}{S_{\ell c}} \int c_s c \, dy$	distance from vortex force centroid to the leading edge
S	reference area
$S_{12}(r_1, r_2, \omega)$	cross power spectral density of pressures at r_1 and r_2
$S_{\ell e}$	length of the leading edge
$S(\omega)$	power spectral density
$S_w(\omega)$	power spectral density of total displacement
$S_q(\omega)$	power spectral density of buffeting response
$S_{BM}(\omega)$	power spectral density of root bending moment
$S_{\overline{Qn}}$	power spectral density of the buffeting excitation
V_∞	free stream velocity
$V' = \frac{1}{2} V_\infty$	vortex-induced normal velocity
V	tunnel flow velocity
W	tunnel width
$w_{\ell e}$	normal velocity at the leading edge
$\bar{y}_\ell$	distance from apex to centroid of $\underline{c_s}$ distribution from inboard to η of $c_{s(max)}$, measured along the leading edge and referred to half span
$z_a(x,y,t)$	structural displacement
$\overline{z_a^2}$	mean square value of displacement

$Z_{nj}(\omega)$	the complex impedance of the system
Z^{-1}	the inverse of $z_{nj}(\omega)$, or the structural transfer function
α	angle of attack
α_{BD}	α for vortex breakdown at the trailing edge in symmetrical loading
$\Delta\alpha$	$= \alpha - \alpha_{BD}$
ζ_a	aerodynamic damping ratio
ζ_s	structural damping ratio
ζ	total damping ratio, aerodynamic and structural
ρ	free stream density
ω	angular frequency, $2\pi f$
ω_n	natural frequency of the system
$\phi_n(x,y)$	normal mode shapes of the system
Γ	sectional curculation
Γ_t	total buffeting vortex strength
$\overline{\Gamma}_t$	total buffeting vortex strength per unit length of the leading edge
$\overline{\Gamma}_s$	steady vortex strength per unit length of the leading edge
AMPLG	buffeting excitation
RMS, rms	root mean square

1. INTRODUCTION

Buffeting flow arises when flow separation occurs on an airplane. The resulting flow field is highly turbulent, thus producing fluctuating pressures on lifting surfaces in the detached flow region. Boundary layer separation is perhaps the most common source producing buffet on most conventional configurations. Research in this area has been quite extensive and involved measurements of fluctuating pressures on models together with some theoretical methods to extrapolate these results to full-scale vehicles (see, for example, Refs. 1-3). Frequently, these pressure measurements are made on a conventional "rigid" model, instead of an aeroelastic one, because the latter may not be able to withstand high enough dynamic pressures to be realistic. Based on this consideration, several theoretical methods to use these pressure measurements to predict buffet response have been developed. Some of these methods will be reviewed later. Review of some test results can be found in References 4 and 5; and of theoretical methods, in References 6 and 7.

Of particular interest in the present investigation is the buffeting caused by leading-edge vortices on slender wings. Test results showed that

(1) buffeting was low before vortex breakdown and became severe after that (Refs. 8 and 9);

(2) low-frequency buffeting was more severe (Ref. 8);

(3) high-frequency buffeting was caused by boundary layer fluctuation, and leading-edge vortices produced mainly low-frequency fluctuation (Ref. 10);

(4) the results were not sensitive to Reynolds numbers (Refs. 10 and 11), so that flight and tunnel measurements could be well correlated (Ref. 12);

(5) buffeting at vortex breakdown was associated with the wing response at the fundamental mode (Ref. 8).

One conclusion from this early-day research on leading-edge vortices was that the buffeting induced by vortex breakdown would mostly be academic because a slender-wing airplane would normally not operate in the vortex-breakdown region of angles of attack. Investigation on the effect of vortex breakdown on the buffeting of nearby lifting surfaces, such as tails, was scarce. However, it is known that the vortex from the strake (or leading-edge extension, LEX) may reduce the buffet intensity on the wing before it bursts (p. 109, Ref. 7).

In the present study, the main objective is to predict buffeting on vertical tails induced by LEX vortex bursting. Fundamental equations for structural response will first be derived. Existing theoretical methods for buffet prediction will be reviewed. The present method and some numerical results will then be presented.

In the Appendix, results of water tunnel testing of an F-18 model are described.

2. THEORETICAL DEVELOPMENT

2.1 Formulation of Equations

Structural Equations of Motion:

Let the structural displacement, $z_a(x, y, t)$, be expressed in terms of normal mode shapes, $\phi_n(x, y)$. Then

$$z_a(x, y, t) = \sum_{n=1}^{N} q_n(t)\phi_n(x, y) \tag{1}$$

where $q_n(t)$ is the so-called generalized coordinate . It can be shown that the structural equations of motion in forced oscillation in generalized coordinates can be written as (Ref. 13, pp. 131-139, or Ref. 14, Chapter 10):

$$M_n\ddot{q}_n + M_n\omega_n^2 q_n = Q_n \equiv \iint [p_E + p_M]\phi_n(\xi, \eta)d\xi d\eta \tag{2}$$

where

$M_n = \iint \phi_n^2 m dxdy$, the generalized mass

$m(x, y)$ = mass per unit area

ω_n = frequency of the n^{th} normal mode

Q_n = the generalized force.

The generalized force consists of two terms, one being the externally applied force (i.e., the p_E-term) and the other being the force due to structural motion (i.e., the p_M-term).

The p_M-term can be further decomposed in terms of the generalized coordinates as

$$p_M = \sum_{j=1}^{N} \Delta p_j(x, y; \omega, M_\infty) \frac{q_j}{b_o} \tag{3}$$

where Δp_j is the lifting pressure at point (x, y) on the wing caused by the motion of the j^{th} normal mode and b_o is the reference length, e.g. the root semichord. It follows that

$$Q_{Mn} = \sum_{j=1}^{N} \frac{q_j}{b_o} \iint_{S_w} \Delta p_j \phi_n d\xi d\eta = q_\infty \sum_{j=1}^{N} \frac{q_j}{b_o} \iint_{S_w} \Delta C_{p_j} \phi_n d\xi d\eta$$

$$= b_o \ell \frac{q_\infty}{b_o} \sum_{j=1}^{N} A_{nj} q_j \qquad (4)$$

where A_{nj} is the generalized aerodynamic force matrix and is defined as

$$A_{nj} = \iint \Delta C_{p_j} \phi_n \, d\bar{\xi} d\bar{\eta} \qquad (5)$$

$$\xi = b_o \bar{\xi}$$

$$\eta = \ell \bar{\eta} \qquad (6)$$

In Equation (4), q_∞ is the dynamic pressure ($= \rho V_\infty^2/2$).

Equation (2) can now be written as

$$M_n \ddot{q}_n + M_n \omega_n^2 q_n - \ell q_\infty \sum_{j=1}^{N} A_{nj} q_j = \iint p_E(\xi, \eta, t) \phi_n(\xi, \eta) d\xi d\eta$$

$$= Q_n^E(t) \qquad (7)$$

In the above derivation, neither structural nor viscous dampings have been included. To include the former, ω_n^2 is usually replaced with $\omega_n^2(1 + ig_n)$, where g_n is the structural damping coefficient for the n^{th} mode and is usually taken to be 0.03 if not known experimentally. To account for the latter, $2\zeta M_n \omega_n \dot{q}_n$ is added to the equation with ζ being the damping ratio. Equation (7) becomes

$$M_n\ddot{q}_n + 2\zeta M_n\omega_n\dot{q}_n + M_n\omega_n^2(1 + ig_n)q_n - \ell q_\infty \sum_{j=1}^{N} A_{nj}q_j = Q_n^E(t) \tag{8}$$

Structural Response to Random Excitation:

If the excitation force $Q_n^E(t)$ is random, it may be represented in a Fourier integral (Chapter 14, Ref. 15),

$$Q_n^E(t) = \int_{-\infty}^{\infty} \bar{Q}_n^E(i\omega)e^{i\omega t}d\omega \tag{9}$$

where

$$\bar{Q}_n^E(i\omega) = \lim_{T\to\infty} \frac{1}{2\pi} \int_{-T}^{T} Q_n^E(t)e^{-i\omega t}dt \tag{10}$$

The displacement $q_n(t)$ will also vary randomly, so that a Fourier integral representation is appropriate.

$$q_n(t) = \int_{-\infty}^{\infty} \bar{q}_n(i\omega)e^{i\omega t}d\omega \tag{11}$$

Substituting Equations (9) and (11) into Equation (8), and requiring the relation to be valid for all t, it is obtained that

$$\bar{q}_n(i\omega)[-M_n\omega^2 + 2iM_n\zeta\omega_n\omega + M_n\omega_n^2(1 + ig_n)] - \ell q_\infty \sum_{j=1}^{N} A_{nj}\bar{q}_j = \bar{Q}_n^E(i\omega)$$

or,

$$\sum_{j=1}^{N} \{[-M_n\omega^2 + 2iM_n\zeta\omega_n\omega + M_n\omega_n^2(1 + ig_n)]\delta_{nj} - \ell q_\infty A_{nj}\}\bar{q}_j = \bar{Q}_n^E(i\omega) \qquad , \qquad n = 1,\ldots,N \tag{12}$$

Let

$$Z_{nj}(\omega) = [-M_n\omega^2 + 2iM_n\zeta\omega_n\omega + M_n\omega_n{}^2(1 + ig_n)]\delta_{nj} - \ell q_\infty A_{nj} \tag{13}$$

Note that $Z_{nj}(\omega)$ is called the complex impedance of the system; and its inverse, Z^{-1}, is the so-called structural transfer function.

To describe quantitatively a random response in a meaningful manner, statistical methods must be used. The most important quantity for this purpose is the mean square value. It is defined for a random function F(t) as (Ref. 15)

$$\overline{F^2(t)} = \lim_{T\to\infty} \frac{1}{2T} \int_{-T}^{T} F^2(t)dt = \lim_{T\to\infty} \frac{1}{2T} \int_{-T}^{T} F(t) \int_{-\infty}^{\infty} f(i\omega)e^{i\omega t}d\omega dt$$

$$= \lim_{T\to\infty} \frac{1}{2T} \int_{-\infty}^{\infty} f(i\omega) \int_{-T}^{T} F(t)e^{i\omega t}dtd\omega$$

$$= \lim_{T\to\infty} \frac{1}{2T} \int_{-\infty}^{\infty} f(i\omega)2\pi f^*(i\omega)d\omega = \int_{-\infty}^{\infty} \lim_{T\to\infty} \frac{\pi|f(i\omega)|^2}{T} d\omega \tag{14}$$

where f^* is the complex conjugate of f. Define

$$S(\omega) = \lim_{T\to\infty} \frac{\pi f(i\omega)f^*(i\omega)}{T} \tag{15}$$

Equation (14) becomes

$$\overline{F^2(t)} = \int_{-\infty}^{\infty} S(\omega)d\omega \tag{16}$$

In case the random function depends also on space coordinates, the definition of $S(\omega)$ must be modified. For the generalized force of the n^{th} mode, $Q_n{}^E(t)$, it is defined as (Equation 7)

$$Q_n^E(t) = \iint p_E(r, t)\phi_n(r)dA \tag{17}$$

where space coordinates (ξ, η) are now represented by r. The Fourier spectrum of Q_n^E is

$$\bar{Q}_n^E(i\omega) = \iint \bar{p}_E(i\omega)\phi_n(r)dA \tag{18}$$

The power spectrum of the n^{th} generalized force is given by

$$S_n(\omega) = \lim_{T\to\infty} \frac{\pi}{T} \bar{Q}_n^E(i\omega)\bar{Q}_n^{*E}(i\omega)$$

$$= \lim_{T\to\infty} \frac{\pi}{T} \int_A \bar{p}_E(i\omega)\phi_n(r_1)dA_1 \int_A \bar{p}^*(i\omega)\phi_n(r_2)dA_2$$

$$= \lim_{T\to\infty} \frac{\pi}{T} \iint_{AA} \phi_n(r_1)\phi_n(r_2) \frac{1}{4\pi^2} \int_{-T}^{T}\int_{-T}^{T} p_E(r_1, t_1)p_E(r_2, t_2)$$

$$\cdot e^{i\omega(t_1-t_2)} dt_1dt_2dA_1dA_2 \tag{19}$$

Let $t_2 - t_1 = \tau$. Equation (19) can be written as

$$S_n(\omega) = \iint_{AA} \phi_n(r_1)\phi_n(r_2) \lim_{T\to\infty} \frac{1}{T}\frac{1}{4\pi} \int_{-T}^{T}\int_{-T}^{T} p_E(r_1, t_1)p_E(r_2, t_1 + \tau)$$

$$\cdot e^{-i\omega\tau} dt_1 d\tau dA_1 dA_2$$

$$= \iint_{AA} \phi_n(r_1)\phi_n(r_2) \int_{-\infty}^{\infty} \frac{1}{2\pi} R_{12}(r_1, r_2, \tau)e^{-i\omega\tau} d\tau dA_1 dA_2 \tag{20}$$

where

$$R_{12}(r_1, r_2, \tau) = \lim_{T\to\infty} \frac{1}{2T} \int_{-T}^{T} p_E(r_1, t_1)p_E(r_2, t_1 + \tau)dt_1 \tag{21}$$

is known as the space-time correlation or cross correlation

function. Define

$$S_{12}(r_1, r_2, \omega) = \frac{1}{2\pi} \int_{-\infty}^{\infty} R_{12}(r_1, r_2, \tau) e^{-i\omega\tau} d\tau \tag{22}$$

the cross power spectral density of pressures at r_1 and r_2. It follows that

$$S_n(\omega) = \int_A \phi_n(r_1) \int_A \phi_n(r_2) S_{12}(r_1, r_2, \omega) dA_2 dA_1 \tag{23}$$

$S(\omega)$ or $S_n(\omega)$ is known as the power spectral density. This is because if $F(t)$ were a current, the power developed by this current as it passed through a resistance of one ohm would be $F^2(t)$.

Returning to calculation of the total response, Equations (11) - (13) show that the amplitude of the motion in the n^{th} mode is

$$q_n(t) = \int_{-\infty}^{\infty} \left([Z(\omega)]^{-1} \{\bar{Q}^E(i\omega)\} \right)_n e^{i\omega t} d\omega \tag{24}$$

The total displacement is therefore

$$z_a(x, y, t) = \sum_{n=1}^{N} \int_{-\infty}^{\infty} \left([Z(\omega)]^{-1} \{\bar{Q}^E(i\omega)\} \right)_n \phi_n(x, y) e^{i\omega t} d\omega \tag{25}$$

from which the Fourier spectrum of the total displacement can be identified as

$$\sum_{n=1}^{N} \left([Z(\omega)]^{-1} \{\bar{Q}^E(i\omega)\} \right)_n \phi_n(x, y) \tag{26}$$

and the corresponding power spectrum is

$$S_w(\omega) = \lim_{T \to \infty} \frac{\pi}{T} \left\{ \sum_{n=1}^{N} \left([Z(\omega)]^{-1} \{\bar{Q}^E(i\omega)\} \right)_n \phi_n(x, y) \right\} \left\{ \sum_{n=1}^{N} \left([Z(\omega)]^{-1} \{\bar{Q}^E(i\omega)\} \right)_n^* \phi_n(x, y) \right\} \tag{27}$$

Once $S_w(\omega)$ is known, the mean square value of displacement can be obtained as

$$\overline{z_a^2} = \int_{-\infty}^{\infty} S_w(\omega)d\omega \tag{28}$$

Responses in accelerations, loads, moments, and stresses, etc., can be similarly formulated.

Equation (27) is difficult to simplify because of mode coupling through the generalized aerodynamic force matrix, A_{nj}. If the aerodynamic force due to structural motion is ignored, or $A_{nj} \approx 0$ if $n \neq j$, then Equation (27) can be further simplified. Let

$$Z_{nn}(\omega) = M_n[-\omega^2 + 2i\zeta\omega_n\omega + \omega_n^2(1 + ig_n)] - \ell q_\infty A_{nn} \tag{29}$$

Equation (27) can be rewritten as

$$S_w(\omega) = \lim_{T\to\infty} \frac{\pi}{T} \left\{ \sum_{n=1}^{N} \frac{\bar{Q}_n^E(i\omega)\phi_n(x, y)}{Z_{nn}(\omega)} \right\} \left\{ \sum_{n=1}^{N} \frac{\bar{Q}_n^{*E}(i\omega)\phi_n(x, y)}{Z_{nn}^*(\omega)} \right\} \tag{30}$$

After multiplying this out, it can be obtained that

$$\begin{aligned} S_w(\omega) = \lim_{T\to\infty} \frac{\pi}{T} \Bigg\{ & \sum_{n=1}^{N} \frac{\bar{Q}_n^E \bar{Q}_n^{E*} \phi_n^2(x, y)}{Z_{nn} Z_{nn}^*} + \\ & + \sum_{\substack{j=1 \\ j\neq\ell}}^{N} \sum_{\ell=1}^{N} \frac{\bar{Q}_j^E \bar{Q}_\ell^{*E}}{Z_{jj} Z_{\ell\ell}^*} \phi_j \phi_\ell \Bigg\} \\ = & \sum_{n=1}^{N} \frac{\phi_n^2(x, y)}{|Z_{nn}(\omega)|^2} \int_A \phi_n(r_1) \int_A \phi_n(r_2) S_{12}(r_1, r_2, \omega) dA_2 dA_1 + \\ & + \sum_{\substack{j=1 \\ j\neq\ell}}^{N} \sum_{\ell=1}^{N} \frac{\phi_j(x,y)\phi_\ell(x, y)}{Z_{jj}(\omega) Z_{\ell\ell}^*(\omega)} \int_A \phi_j(r_1) \int_A \phi_\ell(r_2) S_{12}(r_1, r_2, \omega) dA_2 dA_1 \end{aligned} \tag{31}$$

The first series of Equation (31) represents the sum of the spectra of the responses in individual modes. The second series represents the correlation between the responses in different modes. The second series can be ignored if only two or three modes are present and their natural frequencies are widely separated (Ref. 15).

In Reference 16, the cross power spectral density was specified in exponential functions with coefficients determined by experiment.

2.2 Existing Theoretical Methods for Buffet Prediction

All existing theoretical methods require some types of experimental data to work with. Sophistication of these required data distinguishes one method from the other.

Cunningham and Benepe (Refs. 17 and 18):

Pressure power spectral densities are first converted into pressure distributions over the wing for each frequency. The doublet lattice method (DLM) is then used to calculate induced pressures on the tail due to downwash produced by the wing buffet pressures. The wing and tail pressures are used in the DLM to calculate the generalized aerodynamic forces. The whole equation (12) is used without simplification. The calculation is similar to that for gust response.

B. H. K. Lee (Ref. 19):

Again, Equation (12) is used. However, the cross correlation function S_{12} in Equation (23) is either taken to be constant over an aerodynamic panel or asumed to vary exponentially in space.

Mullans and Lemley (Ref. 20):

The fluctuating pressure on a rigid model is again used to calculate the generalized aerodynamic forces. However, the aerodynamic forces due to wing vibration, i.e. A_{nj}-terms, are ignored.

J. G. Jones (Refs. 21 and 22):

It is assumed that each mode behaves as a single-degree-of-freedom system:

$$M_n\ddot{q}_n + 2M_n\zeta\omega_n\dot{q}_n + M_n\omega_n^2 q_n = Q_n^E(t) \tag{32}$$

The aerodynamic forces due to wing motion are ignored. Applying the Fourier transform to Equation (32), it is obtained that

$$M_n(-\omega^2 + 2i\zeta\omega_n\omega + \omega_n^2)\bar{q}_n = \bar{Q}_n^E(i\omega) \tag{33}$$

Using the definition of power spectral density, Equation (15), the power spectral density of the response can be obtained:

$$S_q(\omega) = \frac{S_{\bar{Q}_n}(\omega)}{M_n^2(-\omega^2 + 2i\zeta\omega_n\omega + \omega_n^2)(-\omega^2 - 2i\zeta\omega_n\omega + \omega_n^2)} \tag{34}$$

The mean square value of q_n is therefore

$$\overline{q_n^2(t)} = \int_{-\infty}^{\infty} S_q(\omega)d\omega$$

$$= \int_{-\infty}^{\infty} \frac{S_{\bar{Q}_n}(\omega)}{M_n^2 H_n(\omega)H_n^*(\omega)}\, d\omega \tag{35}$$

where

$$H_n(\omega) = -\omega^2 + 2i\zeta\omega_n\omega + \omega_n^2 \tag{36}$$

The main contribution to the value of the integral in Equation (35) comes from the peak response at $\omega = \omega_n$. If $S_{\bar{Q}}(\omega)$ is assumed not to vary appreciably in the neighborhood of ω_n, it can be factored out of the integral in Equation (35) and the result integrated analytically based on the residue theorem in the theory of a complex variable. Results are available in Reference 23 (p. 218). Therefore, Equation (35) can be reduced to

$$\overline{q_n^2(t)} \approx \frac{\pi}{2} \frac{S_{\bar{Q}_n}(\omega_n)}{M_n^2 \zeta \omega_n^3} \tag{37}$$

Instead of $\overline{q_n^2(t)}$, Jones determined $\overline{\ddot{q}_n^2}$, the mean square acceleration. Note that the Fourier transform of $\ddot{q}_n$ is

$$\bar{\ddot{q}}_n = (i\omega)^2 \bar{q}_n \tag{38}$$

Therefore,

$$S_q^{\cdot\cdot}(\omega) = \frac{(i\omega)^4 S_{\bar{Q}_n}(\omega)}{M_n^2 H_n(\omega) H_n^*(\omega)} \tag{39}$$

The result for $\overline{\ddot{q}_n^2}$ is (Ref. 21)

$$\overline{\ddot{q}_n^2} \approx \frac{1}{8} \frac{\omega_n}{M_n^2 \zeta} S_{\bar{Q}_n}(\omega_n) \tag{40}$$

Let

$$S_{\bar{Q}_n}(\omega_n) = \frac{E^2 \bar{c}}{V} (q_\infty S)^2 \tag{41}$$

where q_∞ is the freestream dynamic pressure and E^2 is a nondimensional aerodynamic excitation parameter. It follows that

$$E = 2\sqrt{2}\left(\frac{V}{\bar{c}\omega_n}\right)^{1/2}\left(\frac{M_n}{S}\right)\left(\frac{\zeta^{1/2}\ddot{\bar{q}}_n}{q_\infty}\right) \tag{42}$$

$$\ddot{\bar{q}}_n = \frac{1}{2\sqrt{2}}\left(\frac{\bar{c}\omega_n}{V\zeta}\right)^{1/2} E\,\frac{q_\infty S}{M_n} \tag{43}$$

To use Equation (43), the damping ratio (ζ) is needed. It consists of both the structural damping (ζ_s) and the aerodynamic damping (ζ_a). The latter arises from the effective angle of attack due to wing vibration and is given by

$$2M_n\zeta_a\omega_n\dot{q}_n = 2q_\infty SK\,\frac{\dot{q}_n}{V} \tag{44}$$

where K, the aerodynamic damping parameter, is a nondimensional parameter depending on the mode shape, the wing planform, and the sectional lift-curve slope. Equation (44) is assumed applicable to both attached and separated flows. It follows from Equation (44) that

$$\zeta_a = \frac{q_\infty SK}{M_n\omega_n V} \tag{45}$$

$$K = \frac{M_n\omega_n V\zeta_a}{q_\infty S} \tag{46}$$

In Jones' method, both E and K are assumed to be independent of the scale effect. In other words, their values determined from model test can be applied to full-scale airplanes. Practical procedures of applying this method were discussed by Butler and Spavins in Reference 24. They are as follows:

(1) Determine modal frequency ω_n, the mode shape, generalized mass M_n, and structural damping ζ_s from wind-off resonance

tests on model and aircraft. Note that the relevant model mode shape must be approximately correct.

(2) Measure rms acceleration or bending moment $\overline{C_B}$ at a point on the wing, the total damping ζ, flow velocity V, and dynamic pressure q_∞, at a given Mach number and angle of attack in wind-tunnel tests.

(3) Relate $\overline{C_B}$ to $\ddot{\bar{q}}_n$ in generalized coordinates using the mode shape (see Section 2.3).

(4) Calculate E from Equation (42).

(5) Calculate K from Equation (46).

(6) Calculate total damping of aircraft by adding calculated ζ_a from Equation (45) to the measured ζ_s.

(7) Predict rms acceleration or bending moment at a point on the aircraft wing from Equation (43) using the measured aircraft mode shape.

Mabey's Method (Refs. 25 and 26):

This method was developed to determine qualitatively the flight conditions for light, moderate and heavy buffeting for the full-scale aircraft from measurement of wing root bending moment of a conventional wind-tunnel model. It is assumed that the wing responds to buffeting pressures in somewhat the same way as to the wind-tunnel turbulence at the wing fundamental frequency.

Let the tunnel unsteadiness $\sqrt{nF(n)}$ be defined so that the total rms pressure fluctuation coefficient is given by

$$\frac{\overline{p^2}}{q_\infty^2} = \int_{-\infty}^{\infty} [nF(n)] \frac{1}{n} dn \tag{47}$$

where

$n = f_o W/V$

W = tunnel width

f = wing fundamental bending frequency in cycles per second

V = freestream velocity.

Define

$$C_{BB}(M, \alpha) = \text{wing-root strain signal}/q_\infty \tag{48}$$

Before the onset of flow separation on the model, $C_{BB}(M, \alpha)$ has been shown experimentally to be constant equal to $C_{BB}(M, \alpha = 0)$. This is the portion of the model response caused by the tunnel unsteadiness $\sqrt{nF(n)}$. Assume that

$$C_{BB}(M, \alpha = 0°) = K_B\sqrt{nF(n)} \tag{49}$$

where K_B is a scaling factor. Then

$$C_{BB}'(M, \alpha = 0°) = \frac{1}{K_B} C_{BB}(M, \alpha = 0°) = \sqrt{nF(n)} \tag{50}$$

Beyond buffet onset, $C_{BB}(M,\alpha)$ is increased due to wing buffet pressures. Let

$$C_{BB}''(M, \alpha) = [C_{BB}'(M, \alpha)^2 - C_{BB}'(M, \alpha = 0°)^2]^{1/2} \tag{51}$$

The angle of attack at which $C_{BB}''(M, \alpha)$ first differs from zero is the buffet-onset angle. From correlations on nine models of fighter aircraft, the following buffeting criteria were suggested:

Buffet onset	$C_{BB}" = 0$
Light buffeting	$C_{BB}" = 0.004$
Moderate buffeting	$C_{BB}" = 0.008$
Heavy buffeting	$C_{BB}" = 0.016$

Note that in using this method, the total damping of the wing fundamental mode should be relatively constant, independent of wind velocity and density. This is true if models with solid wings of steel or light alloy are used, because in this case the structural damping will predominate. No mass, stiffness (or ω_o) and damping for both models and aicraft are needed. It is useful during comparative tests for projects with alternative wing designs.

Thomas' Method (Ref. 27):

At transonic speeds, buffeting is closely connected with flow separation due to shock-boundary layer interaction and shock oscillations. Using conventional boundary layer methods, the development of boundary layer on airfoils at transonic speeds can be calculated. By comparing calculations with experimental results, Thomas postulated that buffet onset started if the point of rear separation coming from the trailing edge reached 90% of the airfoil chord.

Redeker (Ref. 28) extended this method to infinite yawed wings by using the pressure distribution on a section normal to the leading edge and applying a three-dimensional compressible boundary layer method.

Further extension of Thomas' method to finite wings was made by Proksch (Ref. 28). A buffeting coefficient (C_{Bi}) is defined which is directly related to the rms value of the wing root bending moment. It is assumed that the fluctuations of the wing root bending moment are proportional to the integral evaluated along the wing span of the product of local lift fluctuations and the distance from the wing root ($\eta - \eta_R$). A further assumption is that the local lift oscillations caused by flow separation are proportional to length $\ell_s(\eta)$ of the separated flow at a spanwise station of the wing. It follows that

$$C_{Bi} = \int_{\eta_R}^{1} \frac{\ell_s(\eta)}{\bar{c}} (\eta - \eta_R) d\eta \sim \sqrt{\overline{C_B^{-2}}} \qquad (52)$$

2.3 The Present Proposed Method

Theoretically, it is possible to use Equations (23) - (28) to calculate buffet response in the most general way. However, it would be an expensive undertaking because extensive fluctuating pressure measurement on empennage must be made. In addition, these fluctuating pressures are configuration dependent and vary with flight conditions. Therefore, a method similar to Jones' in structural representation is proposed. That is, the structural motion is assumed to be governed by a single-degree-of-freedom system for each mode (see Equation 32). However, Jones' method is used primarily to extrapolate model test results to full-scale aircraft. On the other hand, in the present method the buffeting

excitation, and hence the generalized aerodynamic force $Q_n^E(t)$, is calculated from given configuration geometry, based on a limited amount of force measurements on delta wings. In this report, only the calculation of buffeting force will be considered. The final solution of Equation (32) and its applications in calculation of root bending moment will be investigated in the future. It should be noted that the proposed method accounts only for buffeting due to vortex breakdown.

In developing the proposed method in calculating the buffeting force, the following steps are needed.

(1) Buffeting vortex strength in the burst region must be known. It is known that steady vortex strength from a slender wing or LEX can be estimated by the method of suction analogy (Ref. 29). Similarly, buffeting vortex strength can also be estimated if buffeting normal force data on slender wings are available. This is because any buffeting on slender wings can be assumed to be caused by the leading edge vortex. A limited amount of such data was published in References 4 and 9.

Let c_s be the sectional suction coefficient. Based on the suction analogy, the vortex lift is proportional to c_s. The vortex lift can also be expressed in terms of the vortex strength Γ through Kutta-Joukowski theorem as

$$\frac{1}{2}\rho V_\infty^2 c_s c\,dy = \rho\Gamma w_{\ell e}\,d\ell \qquad (53)$$

where $w_{\ell e}$ is the normal velocity at the leading edge and $d\ell$ is the vortex length along the leading edge. It follows that

$$\frac{\Gamma}{V_\infty} d\ell = \frac{1}{2} \frac{c_s c}{w_{\ell e}/V_\infty} dy$$

and

$$\Gamma_t = \int \frac{\Gamma}{V_\infty} d\ell = \frac{1}{2} \int_o^{b/2} \frac{c_s c}{w_{\ell e}/V_\infty} dy$$

The average strength per unit length is

$$\bar{\Gamma}_t = \Gamma_t / S_{\ell e} = \frac{1}{2S_{\ell e}} \int_o^{b/2} \frac{c_s c}{w_{\ell e}/V_\infty} dy \qquad (54)$$

where $S_{\ell e}$ is the length of the leading edge. The unsteady aerodynamics program of Reference 30 was revised to calculate $\bar{\Gamma}_t$.

In addition, a line unsteady vortex from the LEX-wing junction is used to generate buffeting flow for vertical tails. This line vortex will produce additional loading, to be called "augmented vortex lift," due to momentum transfer. According to Figure 1(a), if the force due to momentum transfer is equated to the vortex lift through the suction analogy, then

$$\begin{aligned} \int \frac{1}{2} \rho V_\infty^2 c_s c \, dy &= \int \rho \Gamma \, w \, d\ell \\ &= \int \rho V' \left(\vec{V}' \cdot d\vec{A} \right) \\ &\simeq \int 2\rho \left(\frac{1}{2} V_\infty \right) \left(\frac{1}{2} V_\infty \right) d\ell \, \bar{\Gamma}_{av} \end{aligned} \qquad (55)$$

where V' is taken to be $\frac{1}{2} V_\infty$ based on available data (Ref. 31). From Equation (55), it follows that

$$\bar{\Gamma}_{av} = \frac{1}{S_{\ell e}} \int c_s \, c \, dy \qquad (56)$$

The augmented vortex lift on a downstream lifting surface is then given by (see Figure 1(b))

$$\text{Augmented Vortex Lift} = 2 \, \rho\left(\frac{1}{2} V_\infty\right)\left(\frac{1}{2} V_\infty\right) \tilde{c} \, \bar{\Gamma}_{av}$$

$$= \frac{1}{2} \rho \, V_\infty^2 \, 2 \, \bar{\Gamma}_t \left(\frac{w}{V_\infty}\right)_{\ell e} \tilde{c} \qquad (57)$$

In the calculation, the buffeting normal force is obtained by assuming a vertical oscillation of constant amplitude over the region of predicted vortex breakdown. The latter was calculated by a semi-empirical method to interpolate or extrapolate experimental data (Ref. 32). The amplitude was adjusted to match the experimental data on mean square values of fluctuating normal force coefficients given in Reference 9. The resulting unsteady leading-edge suction is then used to calculate the buffeting vortex strength. Unfortunately, only data at a low frequency for some delta wings were measured in Reference 9. On the other hand, the power spectrum over a range of frequencies at the vortex-breakdown angle of attack for the BAC 221 configuration is available (Fig. 24 of Ref. 4). This is illustrated in Figure 2. Unless additional

data are available in the future, for the present purpose the low-frequency data of Reference 9 will be used to derive the buffeting vortex strength for a range of angles of attack. At other frequencies, the power spectrum is assumed to be that for the BAC-221, and the strength will be multiplied by a ratio obtained from data for the BAC 221 in Reference 4.

(2) RMS root bending moment can be calculated as

$$M_o(t) = \int_o^{b/2} [\ell_E(y, t) + \ell_M(y, t) - (\sum_{n=1}^{N} \ddot{q}_n(t)\phi_n(y))m(y)]ydy \tag{58}$$

where ℓ_E is the sectional lift due to external forces, ℓ_M is the sectional lift due to structural motion and the last term is the inertial forces. For a rigid wing, the last two terms can be ignored. In Jones' analysis, ℓ_M was also ignored. Using the notation of Equation (4), ℓ_M can be written as

$$\ell_M(y, t) = q_\infty \sum_{n=1}^{N} \sum_{j=1}^{N} \frac{q_j}{b_o} \int \Delta C_{p_j}(x, y)\, \phi_n(x, y)mdx \tag{59}$$

Let the Fourier transform of $\ell_E(y, t)$ be written as

$$\overline{\ell_E}(y, t) = \sum_{n=1}^{N} \bar{\ell}_{E_n}(y, i\omega)\bar{Q}_n^E(i\omega) \tag{60}$$

where $\bar{\ell}_{E_n}$ is the sectional lift due to a unit generalized force in the n^{th} mode. Applying the Fourier transform to Equation (58), it is obtained that

$$\bar{M}_o(i\omega) = \int_o^{b/2} \left[\sum_{n=1}^{N} \bar{\ell}_{E_n}(y, i\omega) + \frac{\bar{\ell}_M}{\bar{Q}_n^E} + \sum_{n=1}^{N} \frac{\omega^2}{M_n H_n(\omega)} m\phi_n(y) \right] \bar{Q}_n^E y dy$$

$$= \sum_{n=1}^{N} \left[BM_{E_n}(i\omega) + BM_{M_n}(i\omega) + \frac{\omega^2}{M_n H_n(\omega)} \int m\phi_n(y) y \, dy \right] \bar{Q}_n^E$$

$$= H_{BM}(\omega) \bar{Q}_n^E(i\omega) \tag{61}$$

where Equation (33) has been used. $H_{BM}(\omega)$ is the bending moment transfer function and is defined as

$$H_{BM}(\omega) = \sum_{n=1}^{N} \left[BM_{E_n}(i\omega) + BM_{M_n}(i\omega) + \frac{\omega^2}{M_n H_n(\omega)} \int_o^{b/2} m\phi_n(y) y \, dy \right] \tag{62}$$

The power spectral density of $M_o(t)$ is therefore

$$S_{BM}(\omega) = |H_{BM}(\omega)|^2 S_{\bar{Q}_n}(\omega) \tag{63}$$

where $S_{\bar{Q}_n}$ is the power spectral density of the buffeting excitation. For a rigid wing, Equation (63) can be simplified to

$$S_{BM}(\omega) = |BM_E(i\omega)|^2 S_{\bar{Q}_n}(\omega) \tag{64}$$

In applications, BM_E will be calculated by assuming a unit buffeting excitation over the region of vortex breakdown at a range of frequencies. The mean square value of root bending moment is then given by

$$\overline{M_o^2} = \int_{-\infty}^{\infty} S_{BM}(\omega) d\omega = 2 \int_o^{\infty} S_{BM}(\omega) d\omega \tag{65}$$

which is to be integrated numerically.Square root of the integrated value provides the rms value of root bending moment.

(3) Since only total force power spectrum, instead of pressure power spectrum, will be used, it is assumed that the pressure fluctuations at every point on the wing are perfectly correlated in space and are in phase. Based on this assumption, Mabey and Butler showed that the total force power spectral density was proportional to the pressure power spectral density (Ref. 11). The results from this were shown to be reasonably accurate.

In the present application to empennage buffeting due to a LEX vortex, those unstedy buffeting vortices, once generated, will be convected downstream in accordance with the general principle of unsteady aerodynamics.

(4) With the power spectral density of buffeting vortex strength determined at a given flight condition, fluctuating normal velocity will be induced on the empennage. By satisfying the usual flow tangency condition, buffeting pressure spectral density on the empennage can be calculated. From the buffeting pressure spectral density, the power spectrum of bending moment or other aerodynamic characteristics can be determined. The mean square values of root bending moment are calculated by using Equation (65).

(5) Similar to Jones' method, the calculation of buffet response requires structural data, such as mode shapes, generalized mass, and damping ratio. Aerodynamically induced damping can have major effect on buffet response and it must be accounted for in analytical representation of flexible aircraft.

(6) In applications to empennage buffeting, the locations of LEX vortex bursting may be based on experimental data or theoretical calculation (Ref. 32).

3. NUMERICAL RESULTS

Extensive measurements of buffeting normal force were made by Earnshaw and Lawford on a series of delta wings at a low frequency of n = 0.05, where

$$n = f\bar{c}/V_\infty \tag{66}$$

and f is the frequency in cycles per second. "n" is converted into the conventional reduced frequency k by multiplying by 2π. Before vortex breakdown, the normal force fluctuation is assumed to be caused by tunnel flow unsteadiness. At each angle of attack, a buffeting vortex strength $\bar{\Gamma}_t$ can be calculated from Equation (54). The same expression is used to calculate the vortex strength $\bar{\Gamma}_s$ in steady flow using the steady-flow c_s. If the results are plotted in terms of the ratio of buffeting to steady vortex strengths, $R_{b/s}$:

$$R_{b/s} = \bar{\Gamma}_t/\bar{\Gamma}_s \tag{67}$$

curves for cambered and flat wings tend to collapse into a single one. This is illustrated in Figure 3 for a 70-degree delta wing. In Figure 3, $\Delta\alpha$ is the incremental angle of attack beyond that of vortex breakdown at the trailing edge. It follows that the buffeting vortex strength is a function of steady-flow vortex strength and $\Delta\alpha$.

To extend limited available data to different planforms, a correlation parameter capable of correlating vortex-breakdown characteristics is needed. In Reference 32, the nondimensional

distance measured along the leading edge from apex to the centroid of leading-edge suction distribution, $\bar{y}_\ell$, was found to be a useful parameter for this purpose. If this $\bar{y}_\ell$ is used to analyze all experimental data for a series of delta wings in Reference 9, results for buffeting vortex strength can be plotted in one graph as shown in Figure 4. Note that the dash curves in Figure 4 represent extrapolation, because data in that range of $\bar{y}_\ell$-values (i.e. highly swept delta wings or LEX) are not available.

3.1 Results for a 65-degree Delta Wing

To check the theory, test data of Reference 33 for the root bending moment of a 65-degree delta wing will be used. Static bending moment coefficients based on $\bar{c}$ are presented in Figure 5. Calculated results from Reference 29 are also presented for comparison. It is seen that at high angles of attack, the theory overpredicts the root bending moment. The predicted α_{BD} is about 20 degrees, while it is about 18 degrees in the experiment.

To find the buffeting characteristics, it is assumed that the buffeting excitation (i.e. the plunging amplitude in the vortex-breakdown region) for the flat wing is the same as that for a cambered 65-degree delta wing if $R_{b/s}$ is the same. Therefore at a given $\Delta\alpha$, $R_{b/s}$ is obtained from Figure 6. Using this $R_{b/s}$, the buffeting excitation (AMPLG) can be determined from Figure 7. Note that Figure 7 was constructed from the experimental data of

Reference 9 for a cambered wing. The resulting buffeting excitation amplitudes for a flat 65-degree delta wing are plotted in Figure 8.

To calculate the dynamic response of a rigid wing, Equations (64) and (65) will be used. To calculate the transfer function (BM_E) for the root bending moment, a unit amplitude of vertical excitation is prescribed over the region of vortex breakdown at each frequency. Some results are presented in Figure 9. The corresponding power spectral densities for the excitation are obtained by multiplying the values in Figure 8 (for a low frequency only) by a ratio obtained from Figure 2 for other frequencies. The results are shown in Figure 10. Equation (65) is then integrated by the trapezoidal rule to produce the mean square values of root bending moment. The rms values are presented in Figure 11. Note that experimental data were obtained at resonant frequencies of the fundamental bending mode. Since the spectral density is higher at higher frequencies (Fig. 10), the calculated response of a rigid wing tends to be similar to the test data at a high frequency, although the magnitudes are underpredicted. It is expected that the prediction can be improved if the structural flexibility is accounted for.

3.2 Results for an F-18 Configuration

Aerodynamics calculation for an F-18 configuration is based on the code of Reference 29. The modeling of geometry is shown in Figure 12. In the calculation, wing sectional aerodynamic characteristics are needed to account for the effect of viscous

separation at high angles of attack. These characteristics are calculated with Eppler's code (Ref. 34). These calculated results are modified for α beyond the stall α by using experimental data for a flat plate. The strake (i.e. LEX) vortex position and its bursting point can also be calculated and are correlated with water tunnel results in Figure 13. In this calculation, the longitudinal location of vortex bursting point at α = 30 degrees is adjusted to match that from water tunnel results. At other angles of attack, it is determined by extrapolation based on data on bursting progression rates for delta wings (Ref. 32). Additional water tunnel results are presented in the Appendix. The predicted longitudinal characteristics are presented in Figure 14. It is seen that the results are reasonably well predicted.

The calculated LEX vortex position and bursting points at different α's are then used in the unsteady aerodynamics program to calculate the fin buffeting. The buffeting vortex strength is determined from Figure 4. In the calculation, effects of both induced normal velocity from the buffeting vortex and augmented vortex lift are included. The resulting rms values of root bending moment without structural flexibility are presented in Figure 15. Since there are no appropriate test data for comparison, application of Figure 14 is illustrated with the following numerical example. Assume that α = 25 degrees and q_∞ = 30 psf. From Figure 15, $\overline{C}_{Bd}$ is found to be 0.00765. Since the reference length is 11.12 ft. (=b/2) and the reference area is 104 ft^2 (= S_{ref}) for the vertical

tails, it follows that the root mean square value of root bending moment (= $\overline{BM}$) is

$$\overline{BM} = \bar{C}_{Bd}\, q_{\infty}\, S_{ref}\, b/2$$

$$= 0.00765 \times 30 \times 104 \times 11.12 = 265.4 \text{ ft - lb}$$

4. CONCLUSIONS AND RECOMMENDATIONS

Test data showed that vortex breakdown could cause severe buffeting on a lifting surface. In the present investigation, a method was developed to describe buffeting flow after vortex breakdown by interpolating available data through a correlation parameter. The buffeting flow is used as the aerodynamic forcing function to calculate surface pressure distribution and root bending moment through an unsteady lifting-surface theory.

To extend the present work, the following are recommended.

1. The buffeting flow field of a vortex be measured at some axial and circumferential locations. A theoretical method based on statistical concepts, such as those used in inlet dynamic distortion (Refs. 36 and 37), should be developed to describe the buffeting flow field. The latter can be assumed to be independent of tail geometry and is used to generate tail pressure distribution through a lifting surface theory. This approach is different from the conventional method of buffet prediction which requires the measurement of tail surface pressure distribution directly.
2. The simplified aeroelastic model equation (Eq. 32) be solved with the forcing function provided under Task 1. The bending moment is calculated through Equation 58. The combined results of Tasks 1 and 2 should provide a quick estimate of buffeting level on vertical tails when geometry of the latter is changed.

5. REFERENCES

1. Triplett, W. E., "Pressure Measurements on Twin Vertical Tails in Buffeing Flow," Journal of Aircraft, Vol. 20, November 1983, pp. 920-925.

2. Lemley, C. E., and Mullans, R. E., "Buffeting Pressures on a Swept Wing in Transonic Flight--Comparison of Model and Full Scale Measurements," AIAA Paper 73-311.

3. Hwang, C., and Pi, W. S., "Transonic Buffet Behavior of Northropp F-54 Aircraft," AGARD R-624, 1974.

4. Mabey, D. G., "A Review of Some Recent Research on Time-Dependent Aerodynamics," Aeronautical Journal, February 1984, pp. 23-37.

5. Mabey, D. G., "Beyond the Buffet Boundary," Aeronautical Journal, April 1973, pp. 201-214.

6. John, H., "Critical Review of Methods to Predict the Buffet Capability of Aircraft," AGARD R-623, 1974.

7. AGARD AR-82, "The Effects of Buffeting and Other Transonic Phenomena on Maneuvering Combat Aircraft," 1975.

8. Mabey, D. G., "Measurements of Buffeting on Slender Wing Models," British ARC CP-917, March 1966.

9. Earnshaw, P. B., and Lawford, J. A., "Low-Speed Wind-Tunnel Experiments on a Series of Sharp-Edged Delta Wings," British ARC R&M 3424, 1966.

10. Lovell, D. A., and Owen, T. B., "Low-Speed Wind-Tunnel Measurements of Surface Pressure Fluctuations on Two Slender-Wing Models," British ARC C.P. 1154, Sept. 1970.

11. Mabey, D. G., and Butler, G. F., "Measurements of Buffeting on Two 65° Delta Wings of Different Materials," AGARD CP-226, 1977.

12. Rose, R., and Nicholas, O. P., Flight and Tunnel Measurements of Pressure Fluctuations on the Upper Surface of the Wing of a Venom Aircraft with a Sharpened Leading-Edge," British CP 1032, November 1967.

13. Dowell, E. H., Curtiss, H. C., Jr., Scanlan, R. H., and Sisto, F., "A Modern Course in Aeroelasticity," Sijthoff & Noordhoff, 1980.

14. Bisplinghoff, R. L., Ashley, H., and Halfman, R. L., "Aeroelasticity," Addison-Wesley, 1955.

15. Richards, E. J., and Mead, D. J., "Noise and Acoustic Fatigue in Aeronauticas," John Wiley & Sons, 1968.

16. Houbolt, J. C., "Mathematical Modeling and Response Evaluation for the Fluctuating Pressures of Aircraft Buffeting," AGARD-R-630, 1975.

17. Cunningham, A. M., Jr., and Benepe, D. B., Sr., "Prediction of Transonic Aircraft Buffet Response," Paper No. 3 in AGARD-CP-226, Unsteady Airloads in Separated and Transonic Flow, 1977.

18. Cunningham, A. M., Jr., Benepe, D. B., Watts, D., and Waner, P. G., "A Method for Predicting Full Scale Buffet

Response with Rigid Wind Tunnel Model Fluctuating Pressure Data. Volume I: Prediction Method, Development and Assessment," NASA CR 3035, November 1978.

19. Lee, B. H. K., "A Method for Predicting Wing Response to Buffet Loads," Journal of Aircraft, Vol. 21, January 1984, pp. 85-87.

20. Mullans, R. E., and Lemley, C. E., "Buffet Dynamic Loads During Transonic Maneuvers," AFFDL TR-72-46, September 1972.

21. Jones, J. G., "Modelling of Systems with a High Level of Internal Fluctuations," AGARD-CP-172, 1974.

22. Butler, G. F., and Jones, J. G., "The Prediction of Buffeting Response in Flight from Wind-Tunnel Measurements on Models of Conventional Construction," Aeronautical Journal, August/September 1984, pp. 317-325.

23. Gradshteyn, I. S., and Ryzhik, I. M., "Table of Integrals, Series, and Products," Academic Press, 1965.

24. Butler, G. F., and Spavins, G. R., "Preliminary Evaluation of a Technique for Predicting Buffet Loads in Flight from Wind-Tunnel Measurements on Models of Conventional Construction," Paper No. 23, AGARD CP-204, Prediction of Aerodynamic Loading, 1977.

25. Mabey, D. G., "An Hypothesis for the Prediction of Flight Penetration of Wing Buffeting from Dynamic Tests on Wind Tunnel Models," British ARC CP 1171, October 1970.

26. Mabey, D. G., "Prediction of the Severity of Buffeting," Paper No. 7, AGARD-LS-94, Three Dimensional and Unsteady Separation at High Reynolds Numbers, 1978.

27. Thomas, F., and Redeker, G., "A Method for Calculating the Transonic Buffet Boundary Including the Influence of Reynolds Number," AGARD CP-83, 1971.

28. Redeker, G., and Proksch, H. J., "The Prediction of Buffet Onset and Light Buffet by Means of Computational Methods," Paper No. 22, AGARD CP-204, Prediction of Aerodynamic Loading, 1977.

29. Lan, C. E., "VORSTAB--A Computer Program for Calculating Lateral-Directional Stability Derivatives with Vortex Flow Effect," NASA CR-172501, January 1985.

30. Lan, C. E., "The Unsteady Suction Analogy and Applications," AIAA Journal, Vol. 20, December 1982, pp. 1647-1656.

31. Lan, C. E. and Chang, J. F., "Calculation of Vortex Lift Effect for Cambered Wings by the Suction Analogy," NASA CR-3449, July 1981.

32. Lan, C. E., and Hsu, C. H., "Effects of Vortex Breakdown on Longitudinal and Lateral-Directional Aerodynamics of Slender Wings by the Suction Analogy," AIAA Paper 82-1385, 1982.

33. Boyden, R. P., Jr., and Johnson, W. G., Jr., "Results of Buffet Tests in a Cryogenic Wind Tunnel," NASA TM 84520, 1982.

34. Eppler, R., and Somers, D. M., "A Computer Program for the Design and Analysis of Low-Speed Airfoils," NASA TM-80210, 1980.

35. Lutze, F. H., "Curved Flow Wind Tunnel Test of F-18 Aircraft," VPI-Aero-108, April 1980.

36. Melick, H. C. and Ybarra, A. H., "Estimating Maximum Instantaneous Distortion from Inlet Total Pressure RMS and PDS Measurements," NASA TM X-73145, June 1976.

37. Chen, Y. S., "Statistical Prediction of Dynamic Distortion of Inlet Flow Using Minimum Dynamic Measurement - An Application to the Melick Statistical Method," M.S. Thesis, The University of Kansas, 1983.

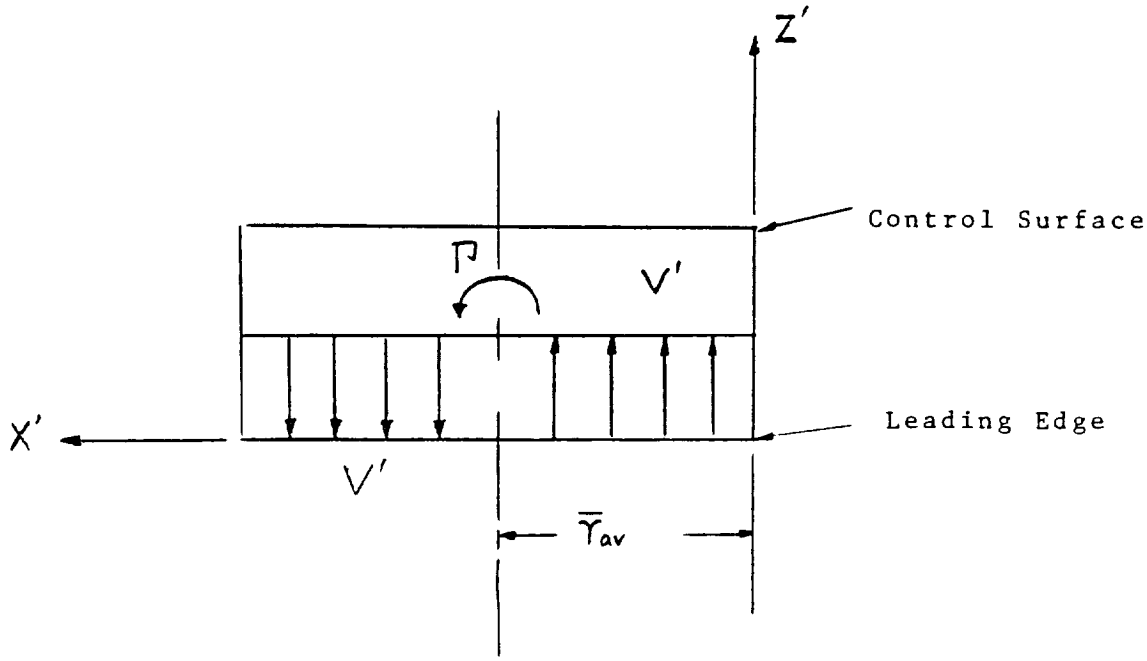

(a) Control Volume to Determine Vortex Centroid Location

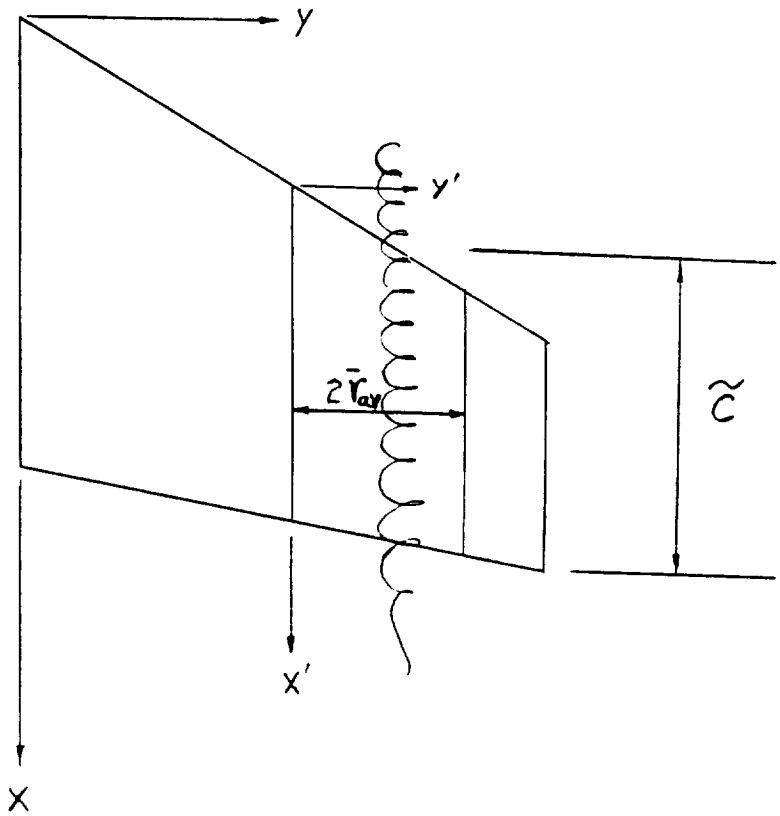

(b) Geometry Characterizing Augmented Vortex Lift

Figure 1. Geometry and Flow Field in Augmented Vortex Lift Concept

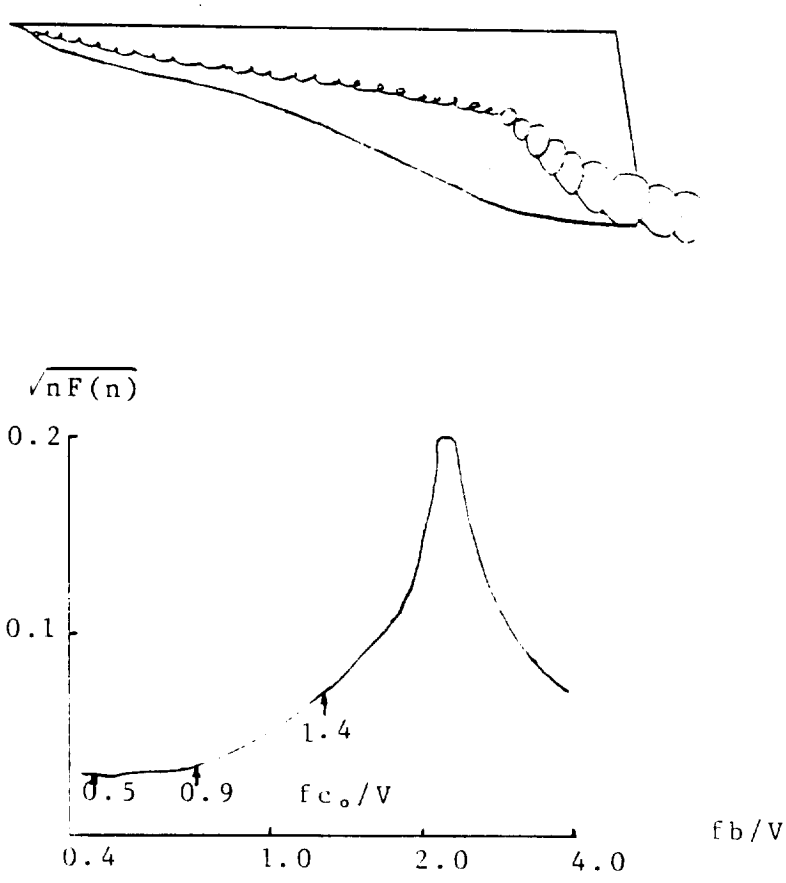

Figure 2. Buffeting Power Spectrum after Vortex Breakdown. Taken from Reference 4.

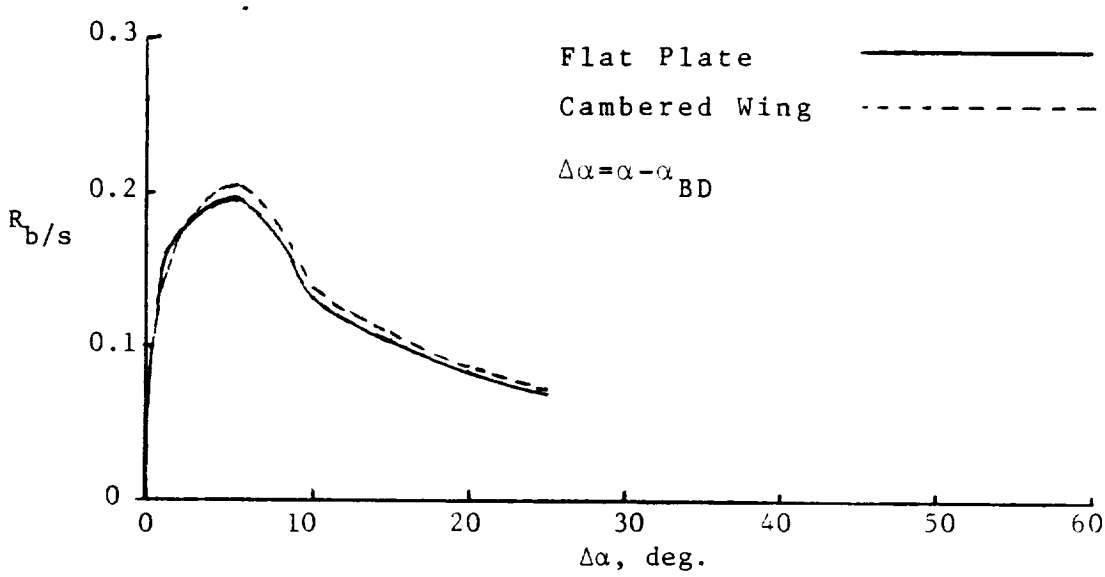

Figure 3. Buffeting Vortex Strength /Steady Vortex Strength versus $\Delta\alpha$ for a 70-deg Delta Wing. n=0.05.

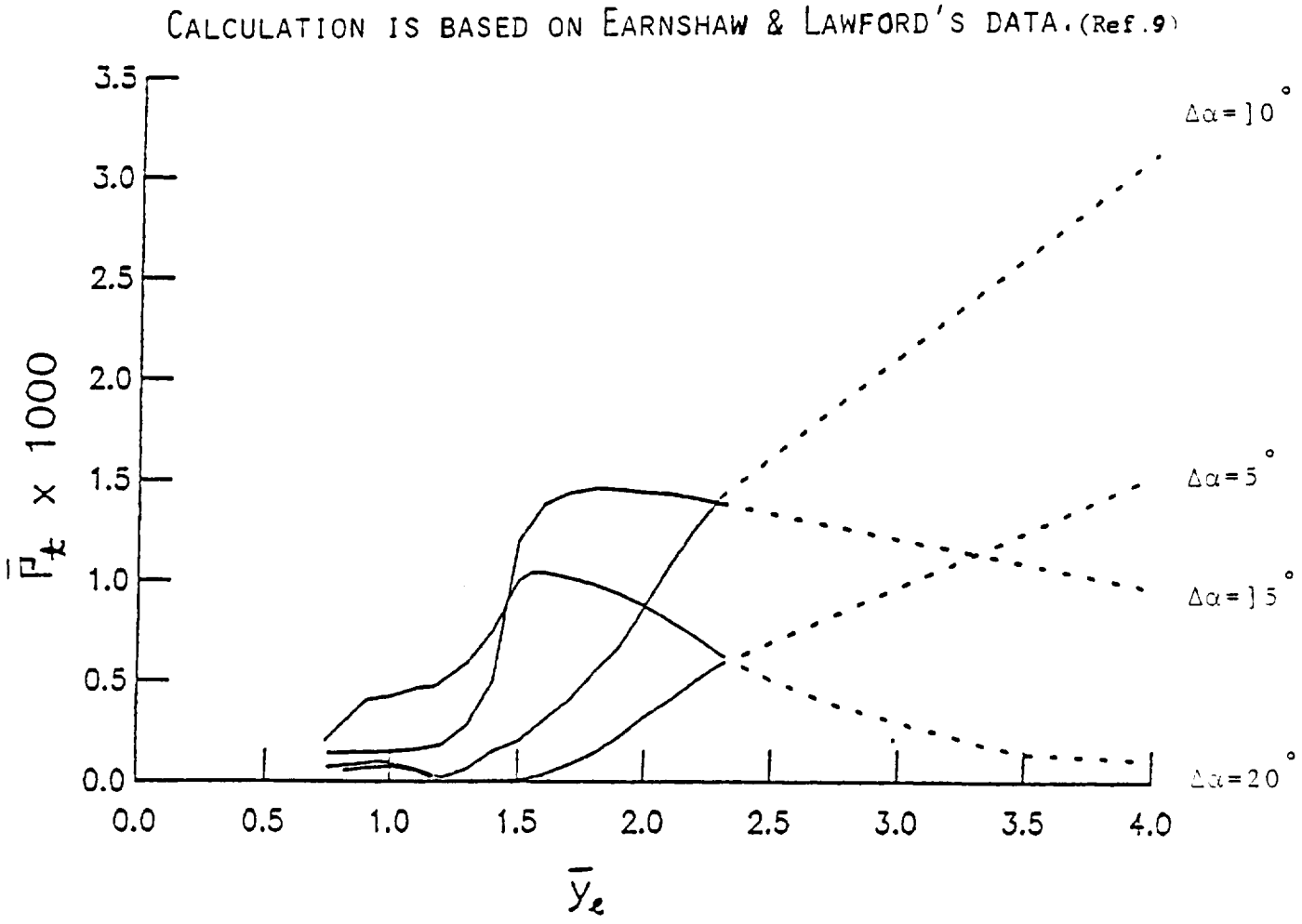

Figure 4. Buffeting Vortex Strength Versus $\bar{y}_\ell$ for Delta Wings. (n=0.05)

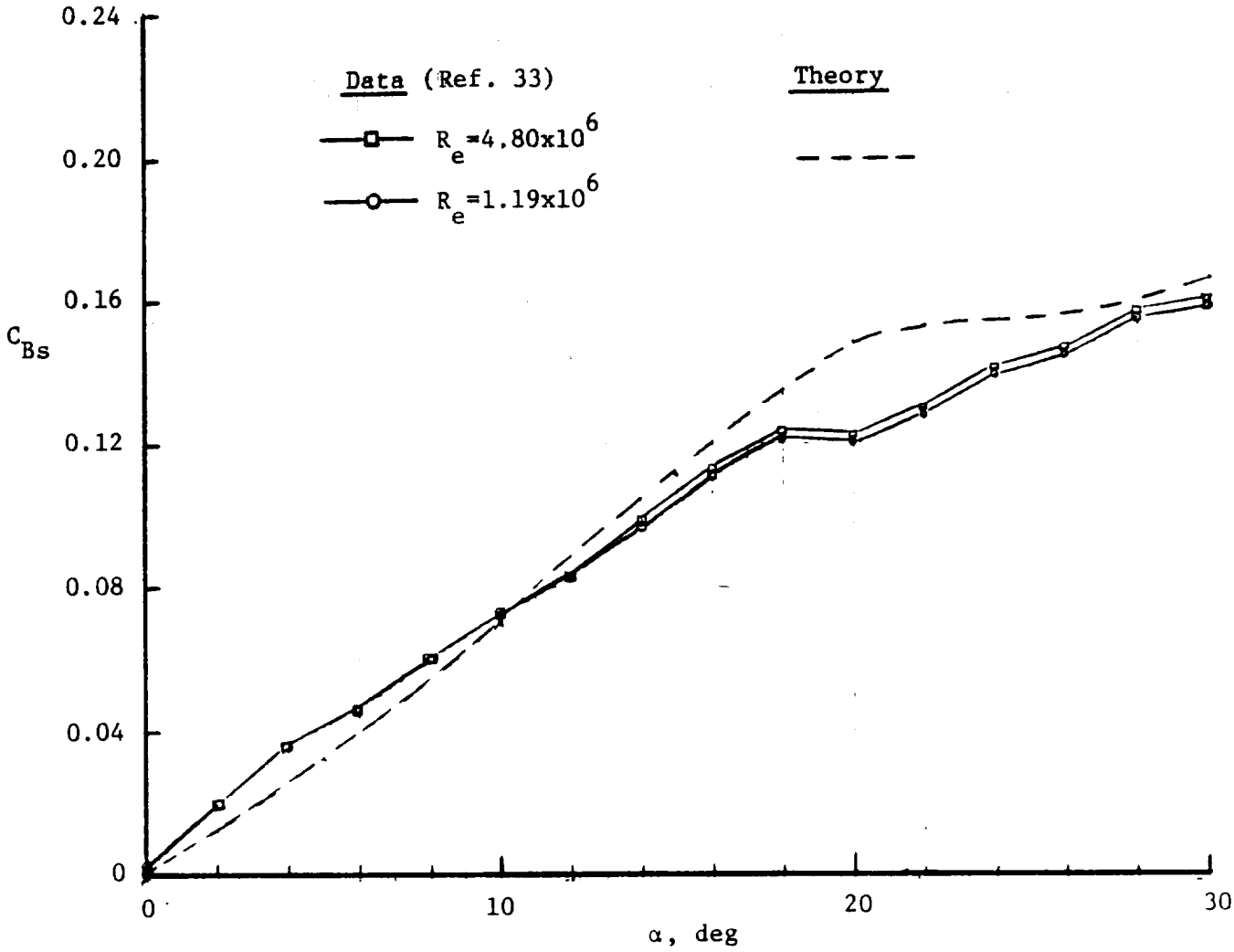

Figure 5. Static Root Bending Moment Coefficient for a 65-deg Delta Wing at M=0.35, C_{B_s} is Based on $\bar{c}$.

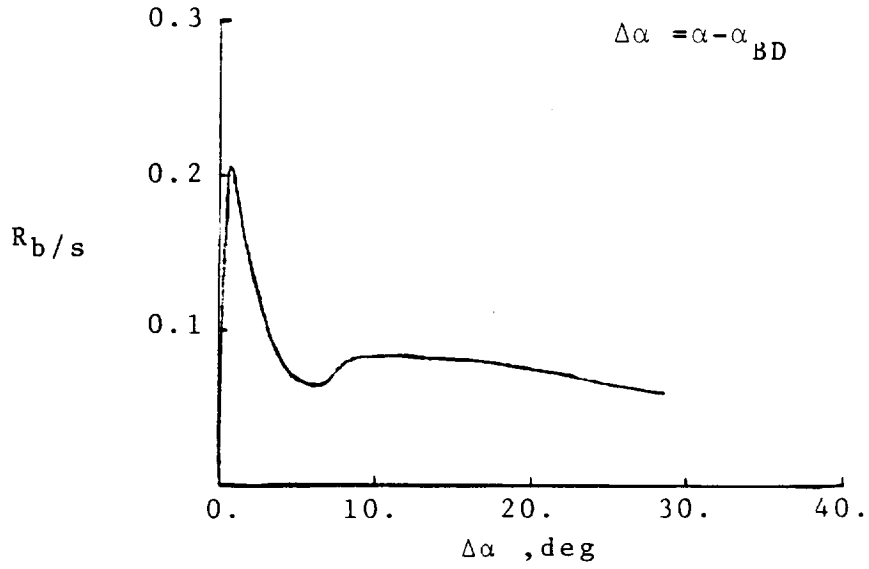

Figure 6. Buffeting Vortex Strength/Steady Vortex Strength vs $\Delta\alpha$ for Λ_{le} =65° Cambered Wing. (n=0.05)

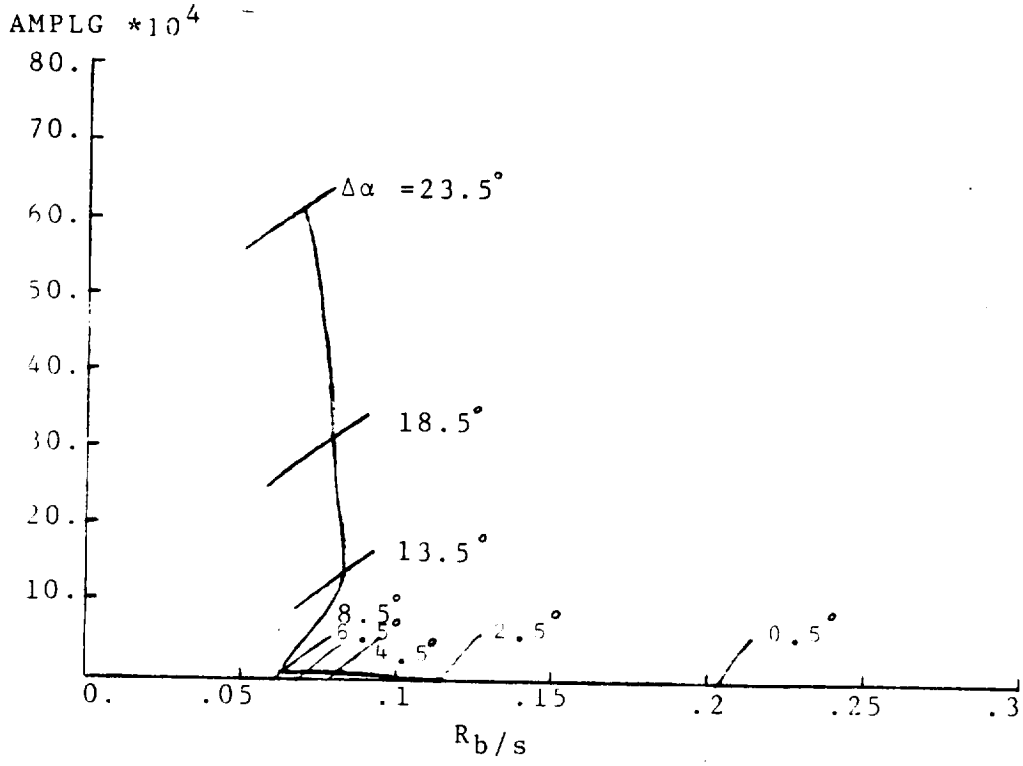

Figure 7. AMPLG vs. $R_{b/s}$ for Λ_{le} =65-deg Cambered Wing. n=0.05.

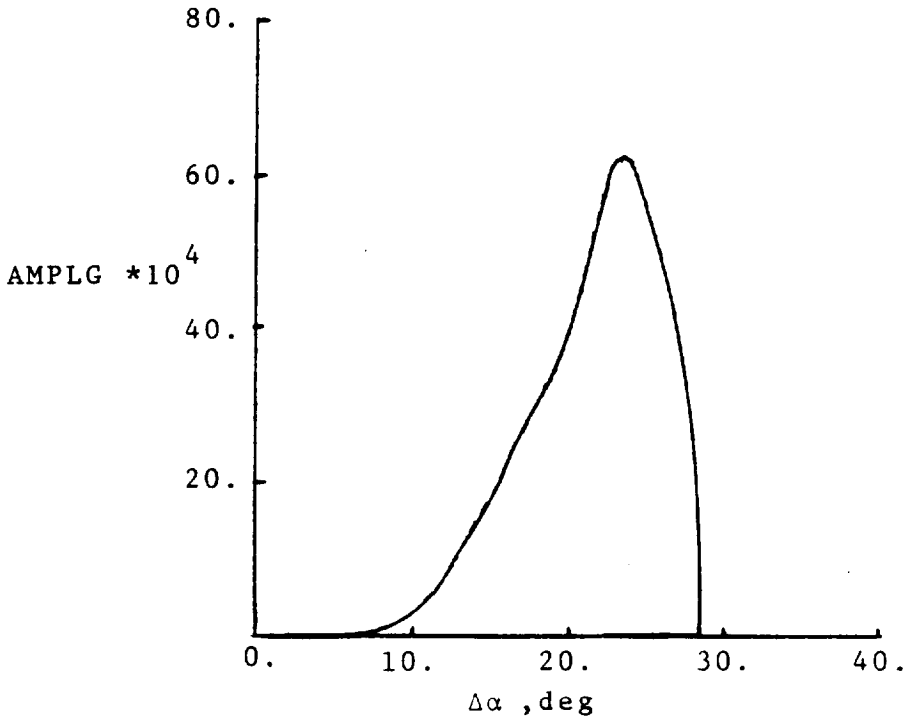

Figure 8. Buffeting Excitation for a 65-deg Flat Delta Wing. n=0.05.

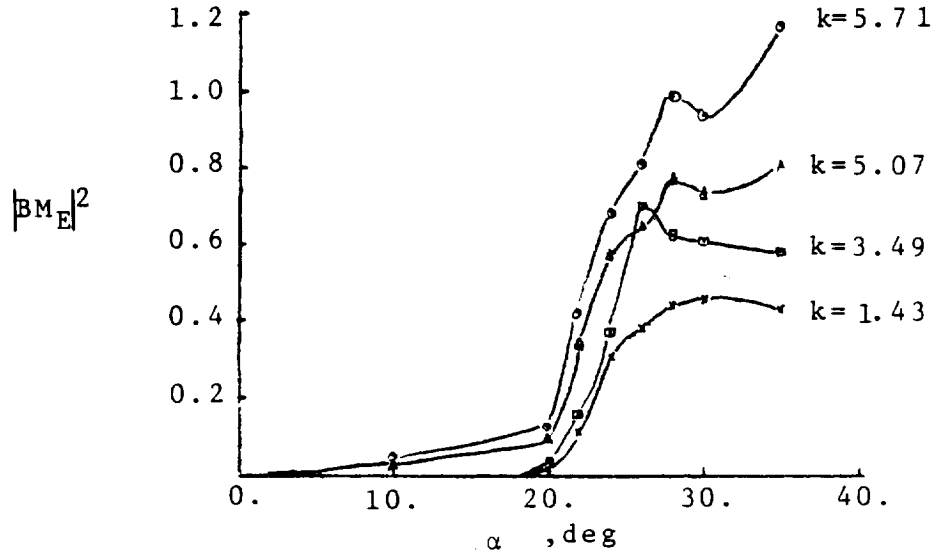

Figure 9. Root Bending Moment Transfer Function for a 65-deg delta Wing.

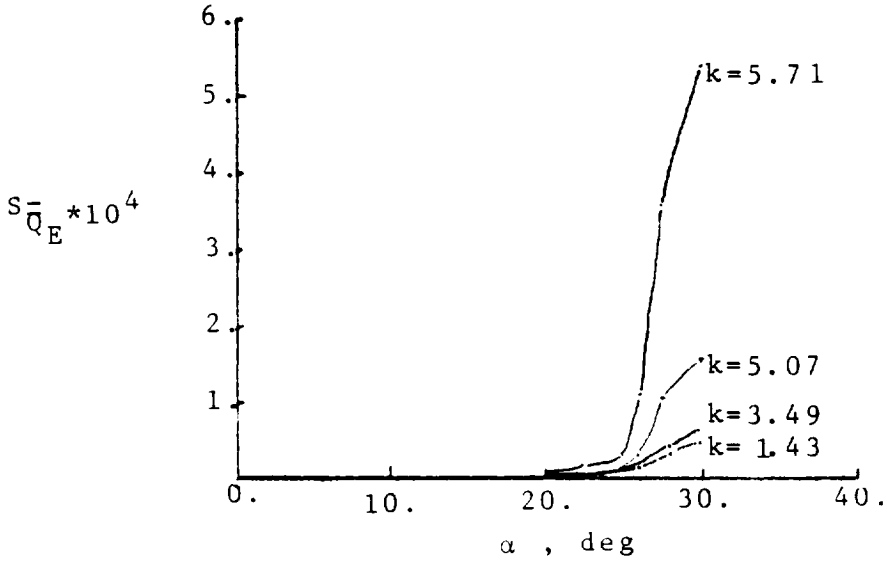

Figure 10. Power Spectral Density of Buffeting Excitation for a 65-deg delta Wing.

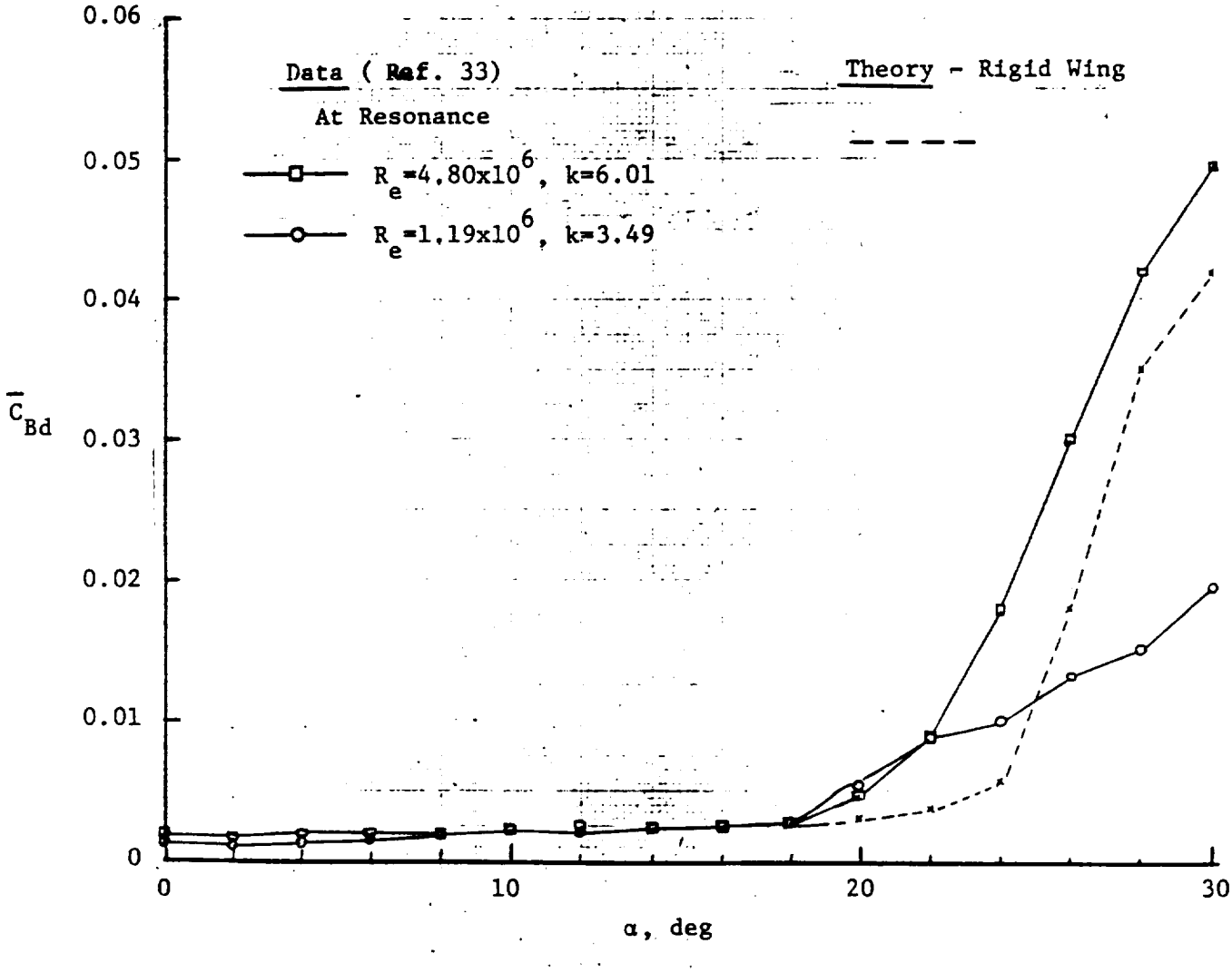

Figure 11. RMS Root Bending Moment Coefficient for a 65-deg Delta Wing at M=0.35, $k=\bar{c}\omega/V_\infty$, $\bar{C}_{Bd}$ is Based on $\bar{c}$.

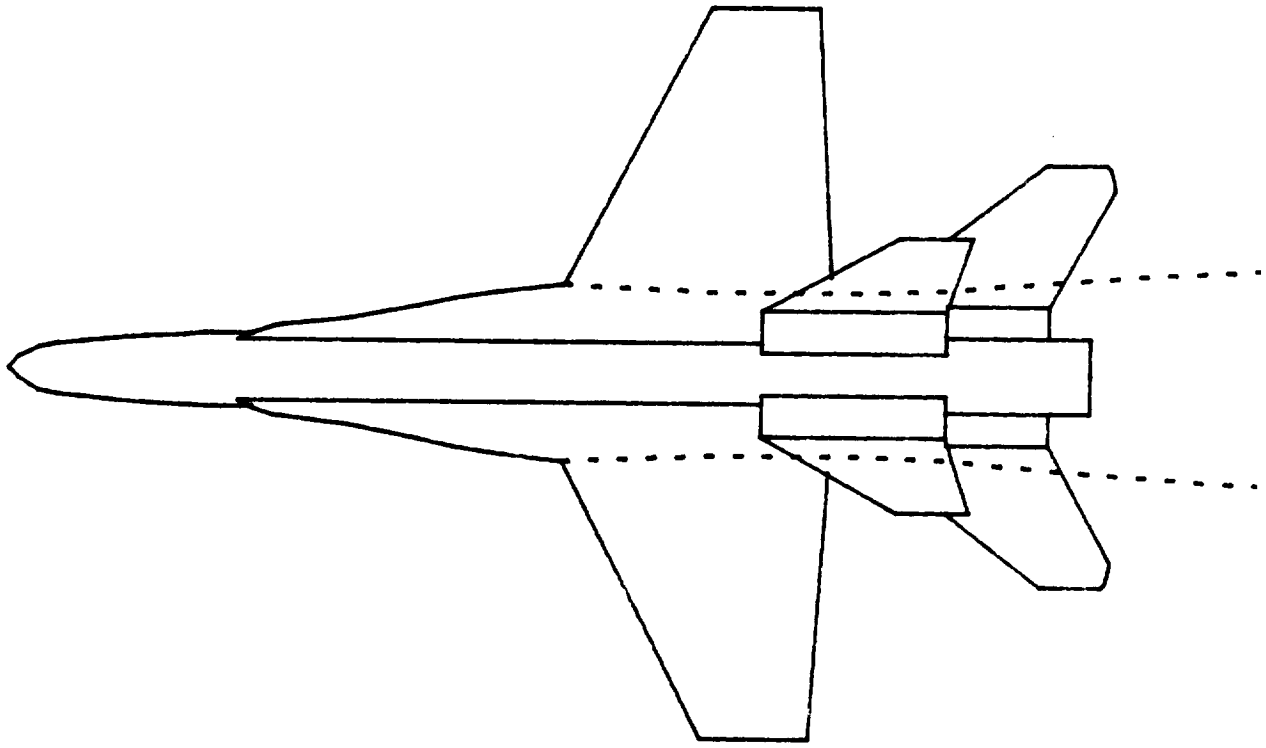

Figure 12. F-18 Geometry Modeling and Strake Vortex Location at alpha=30-deg.

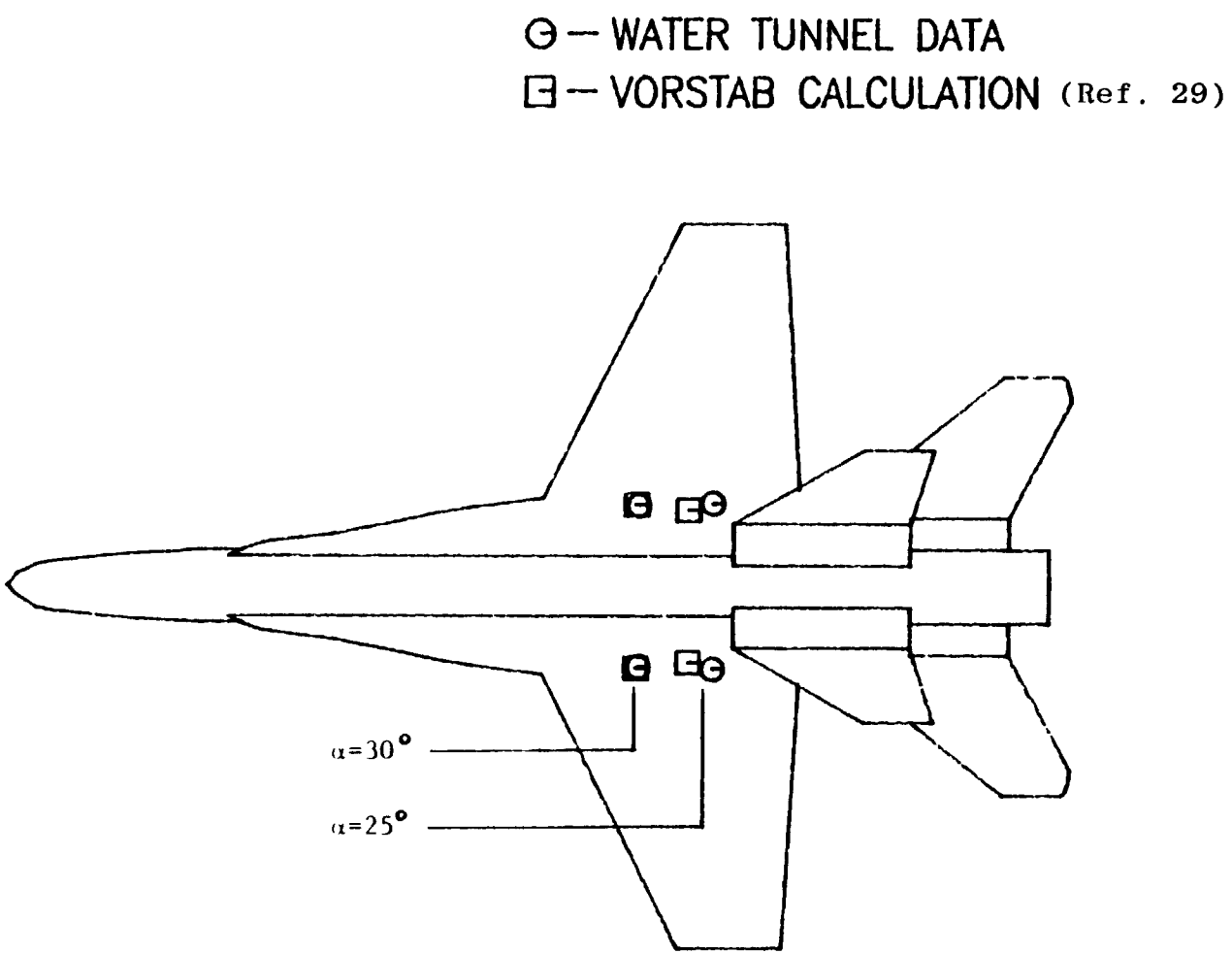

(a) Top view

Figure 13. Locations of Strake Vortex Breakdown for an F-18 Configuration

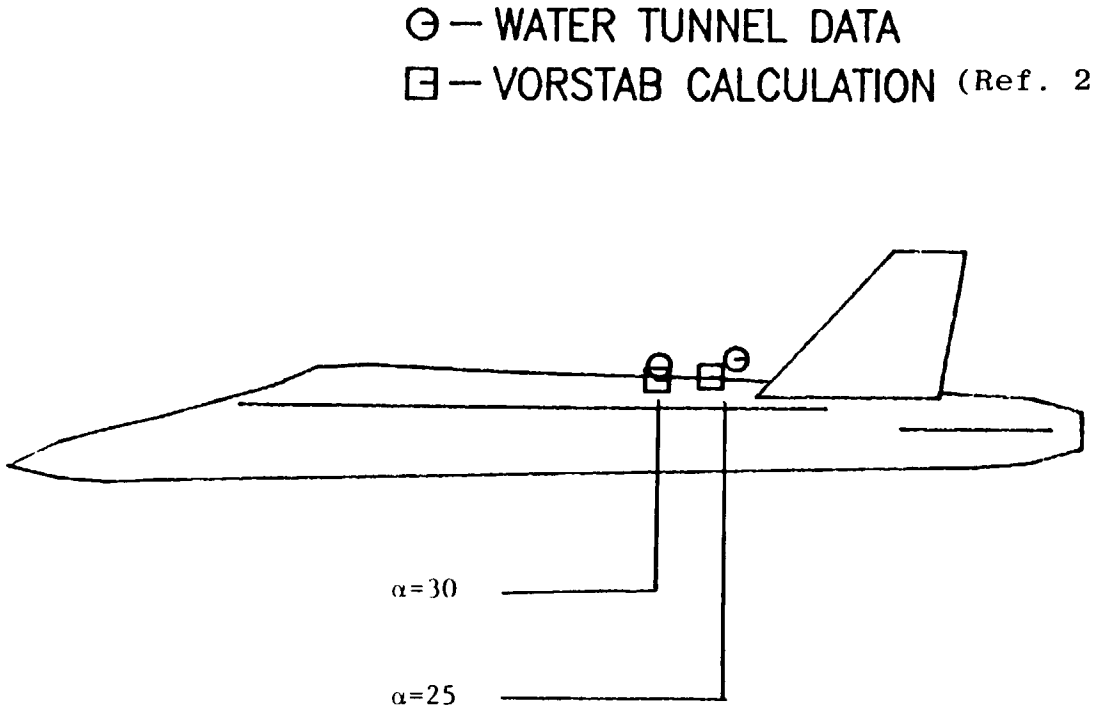

(b) Side view

Figure 13. Concluded.

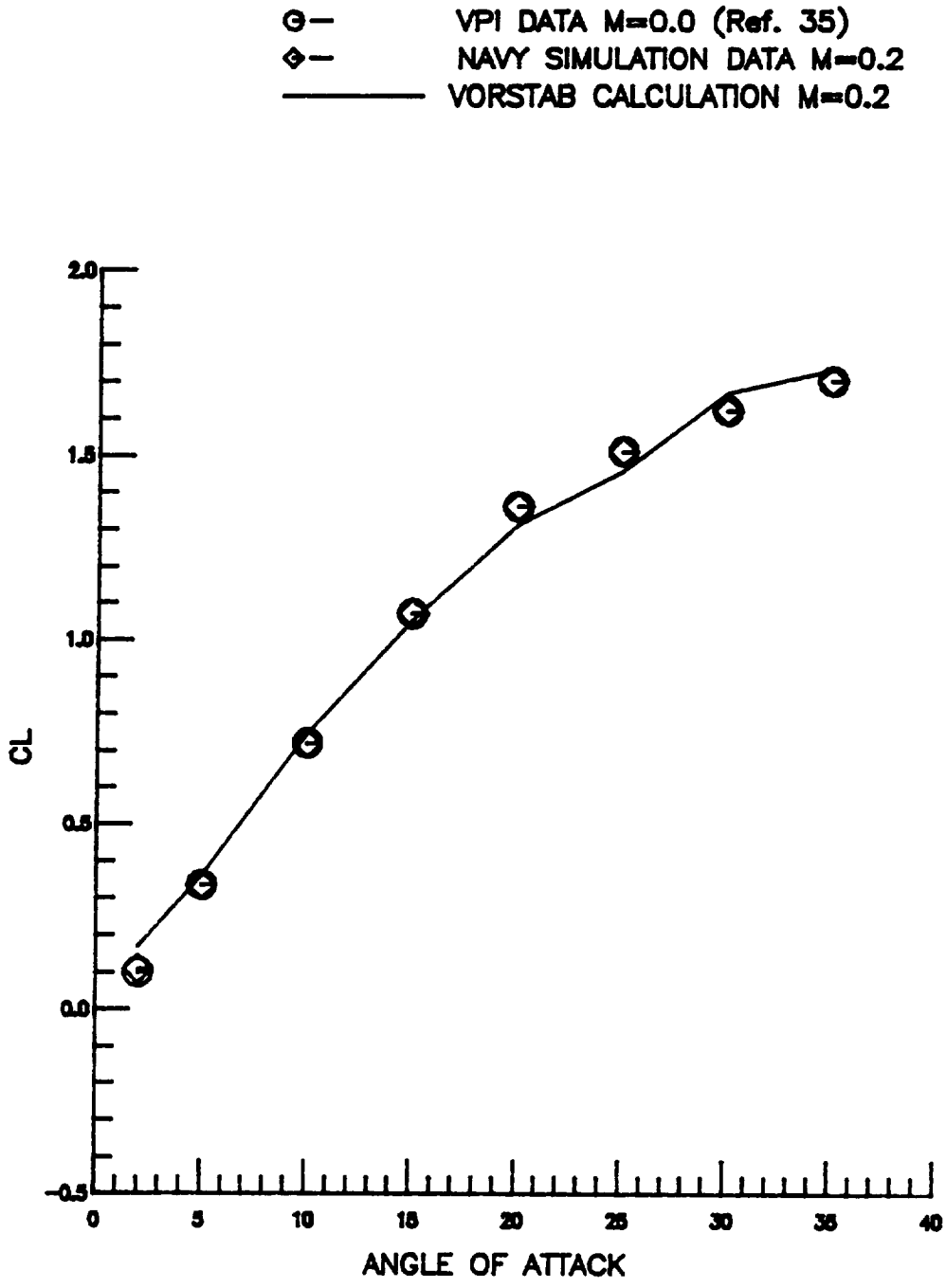

(a) CL vs α

Figure 14. Longitudinal Aerodynamic Characteristics for an F-18 Configuration

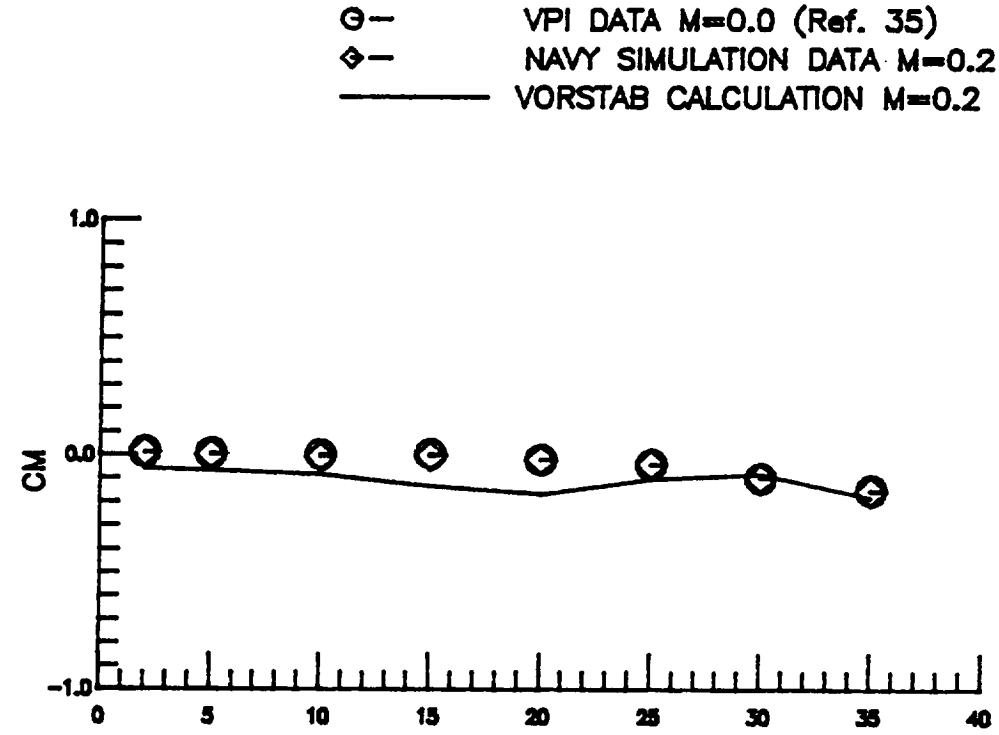

(b) CM vs α

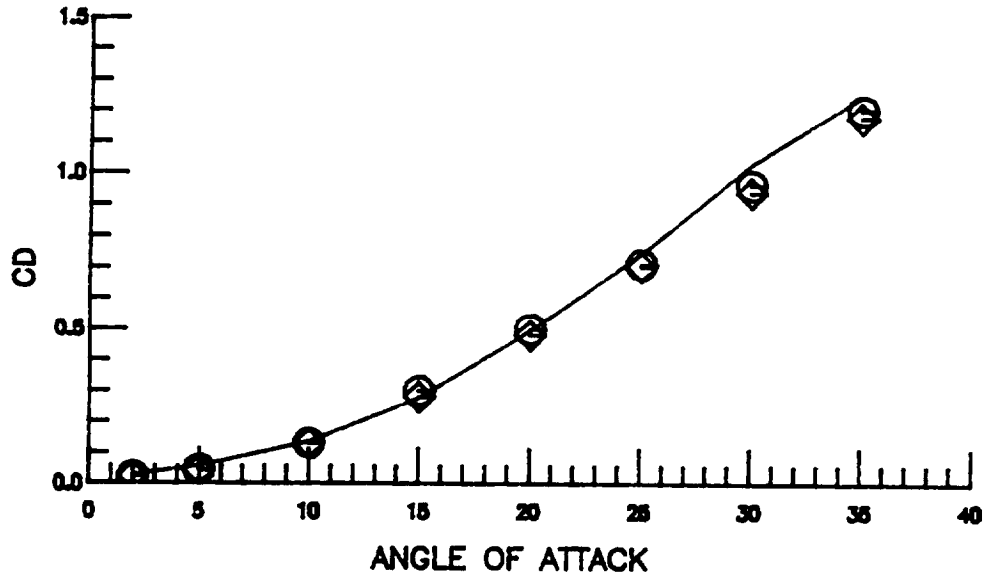

(c) CD vs α

Figure 14. Concluded.

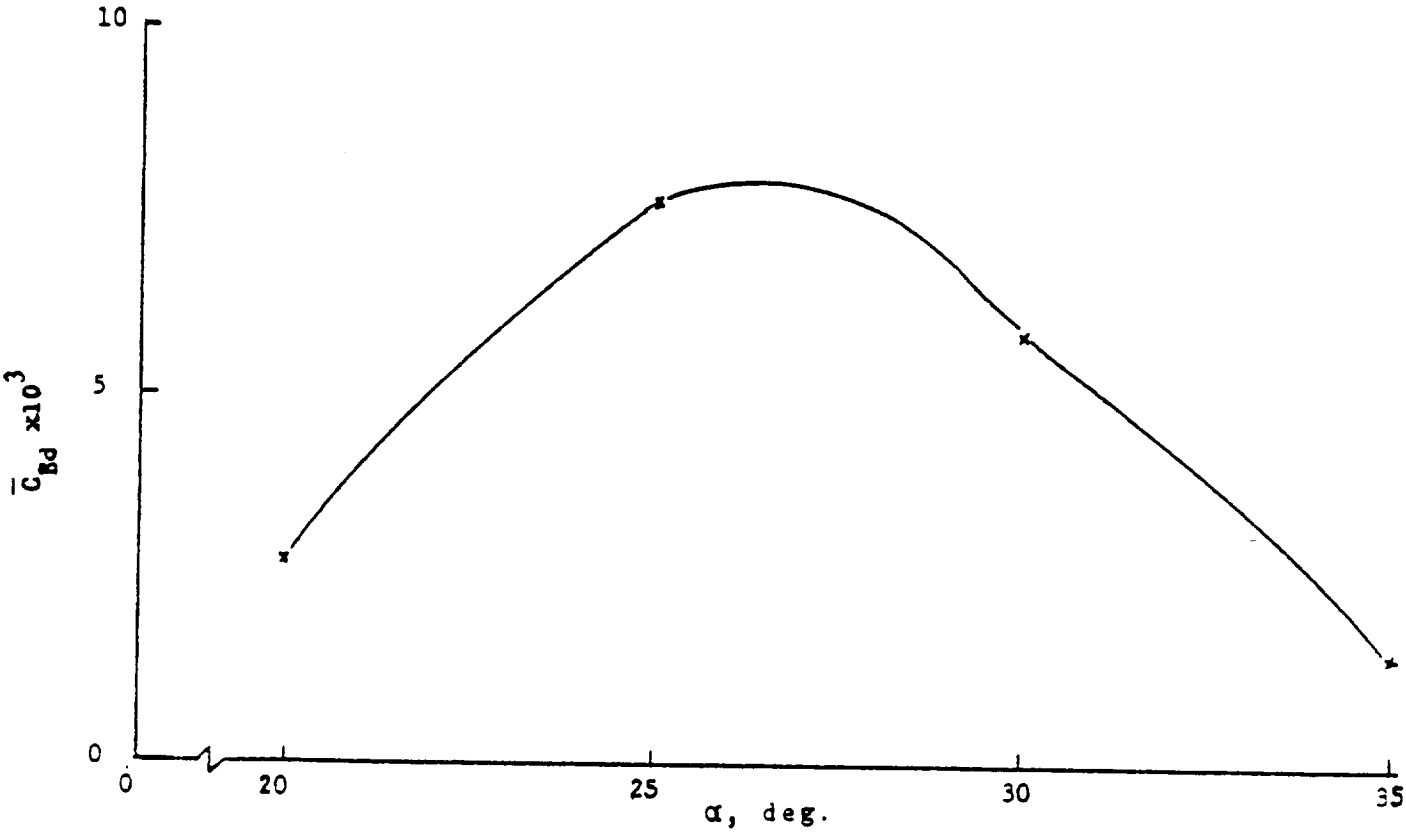

Figure 15. Calculated RMS Root Bending Moment Coefficient for the F-18 Vertical Tail at M=0.0, Rigid Configuration, $\bar{C}_{Bd}$ is Based on b/2 of the Vertical Tail Rotated to the X-Y Plane.

APPENDIX

WATER TUNNEL STUDIES OF VORTEX FLOW AND VORTEX-FIN INTERACTION ON THE F/A-18 AIRCRAFT

BY

WILLIAM H. WENTZ, JR.

Institute for Aviation Research and Development

The Wichita State University

Wichita, Kansas

ABSTRACT

Water tunnel tests have been conducted to study the flow associated with fin buffet for twin-fin fighter aircraft using 1/48th scale F/A-18 models. Flow visualization made use of colored dyes to determine vortex patterns, and surface hot film anemometry was used to study the turbulent energy and the frequencies present in the flow. Configurations tested included the full airplane, airplane without fins, airplane without leading-edge-extensions, (LEX's) and airplane without wings. Test Reynolds number ranged from 4,300 to 12,800, with corresponding Mach numbers less than 10^{-6}.

The flow studies show that the LEX vortices burst just forward of the fins at about 25^{o} angle of attack. Removing the fins had negligible effect on vortex locations and bursting, but removing the wing had a marked effect on both location and burst angle of attack for the vortices. Studies of body vortices with the LEX's removed demonstrated that the body vortices were not a dominant feature of the flow associated with fin buffet.

Hot film anemometer signals show that fin surface turbulence increases with angle of attack, and that dominant frequencies appear in the flow when bursting occurs. The dominant frequencies correspond to a Strouhal number of 0.7 for all speeds tested, and for all angles of attack for which vortex bursting was present. Flow patterns, vortex bursting angles of attack, and Strouhal numbers of the

unsteady flow correlate well with wind tunnel tests from other investigations at higher Reynolds number, confirming the validity of water tunnel testing.

SYMBOLS

c	wing mean aerodynamic chord, (0.24 ft, 1/48th model scale)
f	frequency, Hz
M	Mach number, V/(speed of sound), non-dimensional
Psd	power spectral density of hot film signal, $(\text{Volts})^2/\text{Hz}$
Re	Reynolds number, cV/ν , non-dimensional
S	Strouhal number, fc/V, non-dimensional
V	tunnel velocity, ft/sec
α	angle of attack, degrees
ν	kinematic viscosity, ft^2/sec

INTRODUCTION

Twin-fin arrangements have recently emerged as a configration favored by aircraft designers. This configuration is especially attractive for carrier-based aircraft, since it offers reduced fin height, making hanger access and maintenance easier. The F/A-18 aircraft uses this arrangement, but unfortunately the aircraft has developed fin fatigue problems requiring structural modification. Flight and wind tunnel tests revealed that the un-anticipated fin loads occur at subsonic high angle of attack conditions. These loads are apparently related to the interaction of

vortices emanating from the wing leading edge extensions (LEX's) with the fins.

This report documents tests using small scale models in a water tunnel to visualize the flow phenomena associated with high angle of attack conditions for the twin-fin fighter type aircraft. The primary purpose of this research was to identify the flow associated with fin buffet for this aircraft and to generalize so far as possible from these results, in order to avoid such buffet problems for future designs. A second purpose was to evaluate the water tunnel as a research tool as compared to the more traditional wind tunnel and flight test environments for experimental tests.

EXPERIMENTAL FACILITY

The facility for the experiments reported here was the NASA Ames-Dryden water tunnel flow visualization facility located at Edwards Air Force Base, California. This tunnel is a closed return vertical flow water tunnel, with 16" x 24" test section. Earlier tests of the F/A-18 in a similar water tunnel were reported in reference 1. The tunnel was designed primarily for use as a visualization facility, but in the present tests special surface hot-film anemometry instrumentation was utilized to make quantitative measurements of the unsteady, buffeting flow.

LIMITATIONS OF SMALL-SCALE AERODYNAMIC TESTING

Classical design of fluid dynamic experiments requires "dynamic similarity" of the model and full-scale airplane.

Dynamic similarity is achieved when Reynolds number and Mach number of the model and full-scale airplane are the same, and when the model and full-scale are geometrically similar. In practice, geometric similarity is nearly always achieved by using properly proportioned models. Experiments and theory have shown that matching Mach number is necessary only when compressibility effects become important. This is typically at Mach number above 0.6, depending on thickness ratio. For higher Mach numbers, the pressure distributions are directly affected by compressibility, and Mach matching is essential.

For measurement of skin friction, and precise matching of separation and stalling of airfoils, matching Reynolds number is required. While Reynolds number matching is required in principle, in practice small-scale testing is frequently used, even though it almost always results in Reynolds number below full-scale values. Full-scale, pressurized and cryogenic wind tunnels are facilities in which full-scale Reynolds number is ordinarily achieved. Testing in these facilities is very expensive because of model and operational costs. Fortunately, it is the nature of viscous flow that aerodynamic characteristics are relatively insensitive to Reynolds number. Often Reynolds number differences of factors of 3 or even 10 have relatively small effect on all aerodynamic coefficients except parasite drag and maximum lift coefficients. For the particular case of fighter-type aircraft, which are characterized by thin, highly swept surfaces, operation at low

speed invariably implies high angles of attack, and high angle of attack leads to separation along the leading edges. For such cases, the separation locations are fixed by geometry, and aerodynamic force coefficients and pressure coefficients are essentially independent of Reynolds number. This is borne out by the research of reference 2. It is this peculiar combination of sharp leading edges and high angles of attack that lends validity to small-scale smoke tunnel and water tunnel tests of aircraft designed for supersonic flight. Test planning and interpretation of results must recognize the limitations and the regimes for which testing at Reynolds number substantially lower than full scale may yield useful information.

MODELS

Models were variations of the F/A-18 aircraft, fabricated from 1/48 scale hobby shop kits. The hobby kits are dimensionally sufficiently accurate for tests of this type, so the only modifications required were the addition small-bore tubing to accommodate the dye used for stream tracing, and a mounting strut. Dye tubes were connected to manifolds within the models, which were fed from a separate external dye reservoir for each of the colors desired. In addition, the models were equipped for engine inlet simulation by use of hollow nacelle passages and flexible plastic water siphon tubes attached to the engine exhaust nozzles. By drawing water into the inlets through the siphon tubes at an appropriate rate, it is possible to control the engine mass flow

capture area ratio. This permits proper simulation of streamline patterns around the aircraft. This is particularly important for those regions of flow near the engine inlets, such as the wing leading edges.

Since one purpose of these tests was to evaluate the effects of the various aircraft components on fin buffet, models were designed with several geometric variables. It was less expensive to construct a family of four models with the various configurations than to construct removable hardware for a single model. Wings leading flaps were deflected 34 degrees down, and trailing edge flaps were undeflected for all tests. These settings are consistent with flight at angles of attack 25 degrees and greater. The geometric variables tested are described below.

F/A-18 BASIC MODEL - Complete airplane with leading edge flaps deflected 34 degrees, trailing edge flaps neutral, all tail surfaces neutral.

F/A-18 WITHOUT WINGS - Same as basic model, except wings removed outboard of leading edge extensions (LEX's). This model was used to evaluate the interference effects of the wing and flow fields.

F/A-18 WITHOUT FINS - This model was used to evaluate the possibility that the fin "blockage" might generate an adverse pressure field of sufficient strength to cause premature bursting of the leading edge vortices.

F/A-18 WITHOUT LEX'S - The purpose of this model was to identify the role and interaction of forebody and LEX vor-

tices, and to ascertain possible wing or forebody vortex interactions on the fin.

TEST CONDITIONS

For all tests, inlet flow was established to provide for an inlet capture area ratio of unity. Speed control in the water tunnel is by means of a valve with a series of fixed settings, preventing infinitely variable speed control. Table 1 gives the speeds used for these tests, and corresponding chord Reynolds numbers and Mach numbers.

Table 1 - Test Conditions

Speed (ft/sec)	Reynolds Number	Mach Number
0.25	4,300	0.5×10^{-6}
0.58	9,900	1.3×10^{-6}
0.75	12,800	1.6×10^{-6}

Angle of attack was varied from 0 to 40 degrees, in increments of 5 degrees. At 40 degrees, the model was nearly in contact with the upper wall, so higher angles could not have been tested without the use of an offset sting mount. Video and still pictures were obtained from top and side views in separate runs.

INSTRUMENTATION

Instrumentation consisted of video cassette recording equipment and conventional camera for still photos. In addition, the fin of the basic model was fitted with a strain-gage at the fin root, and two different types of surface hot film anemometers (Disa and Micro-Measurements). These instruments were intended to detect flow unsteadiness over the fin, for correlation with dynamic strain gage data from flight tests.

The Disa hot-film anemometer and the strain gage provided very low-level signals, and these could not be distinguished from random background noise. Only the Micro-Measurements hot film gage provided a signal which displayed characteristics which changed in a consistent manner with angle of attack. Therefore, only the data from the Micro-Measurements hot-film gage was utilized for dynamic measurements. This gage was located at 63% span and 50% chord on the inboard surface of the starboard fin. The output signal from this sensor was monitored on an oscilloscope, and selected signals were also processed using a modal analyzer. The oscilloscope provided real time characteristics of the signal, and the modal analyzer provided frequency analysis of the data in the form of power spectral density (Psd) graphs of the gage voltage. It should be noted that the hot film gage utilized in this manner provides a measure of the heat transfer at the surface. This signal provides a qualitative but not quantitative measure of surface skin friction. The merit in this instrument is the ability to

extract information about the frequencies present in the unsteady flow. Futhermore, these signals can be processed to obtain qualitative differences in turbulent energy levels for the various angles of attack and tunnel speeds.

RESULTS OF FLOW VISUALIZATION

BASIC F/A-18 - The flow video and still pictures show a consistent and repeatable pattern for the vortex flow of this aircraft configuration. Vortex "bursting" or "breakdown" is characterized by an abrupt increase in vortex core diameter, often preceded by a spiralling of the core before complete turbulence ensues. All vortex burst patterns exhibit some unsteadiness, with burst locations oscillating somewhat with time. For this reason, the video images were used as the primary source to determine "average" burst locations. Geometry and vortex burst locations are shown in figure 1. As angle of attack is increased from 0^{o}, vortices form along the LEX's. These vortices increase in strength with angle of attack, and flow aft above the horizontal tail surfaces but beneath the fins for angles below 20^{o}. At 20^{o}, vortex bursting occurs aft of the wing trailing edge and outboard and beneath the fin. At 25^{o} angle of attack, the LEX vortex burst point is located more forward and inboard, with the axis of rotation nearly in line with the fin leading edge. The burst point is slightly forward from the fin leading-edge at this angle of attack. In figure 1 (b), sketches of vortex flow field after bursting are presented to show the proximity of this flow field to the fins. It is difficult to conceive of a vortex burst location which could

be potentially more detrimental in terms of introducing fatigue-producing loads. As angle of attack is increased further, the burst point moves progressively further forward.

F/A-18 WITHOUT FINS - The absence of the fins had negligible effect on the flow field. Vortex locations and burst positions were indistinguishable from the basic model. These results indicate that the pressure gradients associated with the fins are not strong enough to instigate vortex bursting. This is not surprising, considering the small thickness-to-chord ratio of the fins.

F/A-18 WITHOUT WINGS - In this configuration, initial formation of the LEX vortices was in much the same manner as for the full model. As angle of attack was increased, however, the vortices were located more inboard than on the basic model, and they remained intact, without bursting, up to 30° angle of attack. This test series shows important changes in vortex locations and a substantial delay in vortex bursting when the wing is removed. When the wing is present, the adverse pressure gradient field over the aft portion of the wing is evidently a dominant factor in producing vortex bursting.

F/A-18 WITHOUT LEX'S - At high angles of attack, the fuselage forebody, like the LEX's, produces a pair of vortices. This test series shows that the fuselage vortices initially form inboard of the fins, and that they remain inboard of the fins over the entire angle of attack range for which they are visible. At 15° these vortices trail between the fins without bursting. At 20°, bursting occurs

slightly aft of the wing trailing edge, and at 25° the burst location is near wing mid-chord. Burst location remains essentially unchanged as alpha is increased from 25° to 40°. Even at 40°, the spiraling wake of the burst vortices remains close to the fuselage centerline, inboard of the fins. This test series shows that the forebody vortices have much smaller interaction with the fins than the LEX vortices. Studies of the video tapes also show that the spiraling of forebody vortices is at a distinctly lower rate than LEX vortices, indicating lower vorticity associated with the forebody vortices, in agreement with theory.

SUMMARY OF FLOW VISUALIZATION TESTS - Results of the flow visualization test series show that the LEX vortices are the dominant flow feature which provides strong interaction with the fins, and that this interaction is maximum in the 25° to 30° angle of attack range. In this angle of attack range, bursting occurs just ahead of the fin leading edge. Bursting is not influenced by the fins, but is strongly influenced by the presence of the wing.

RESULTS OF HOT-FILM SIGNALS (BASIC MODEL ONLY)

Recently, the "modal analyzer" has been developed for interpretation of dynamic test data, particularly from vibration and flutter testing. This device provides high rate analog-to-digital conversion of signals, with digital storage and processing, including fast Fourier transform techniques (FFT) for determining frequency content of a signal. In addition to its application to strain gage and

accelerometer signals, the modal analyzer is well-suited for analysis of hot film anemometry signals from unsteady or turbulent flows. In the case of fin buffet induced by vortex interactions, it was anticipated that the vortex impingement or vortex bursting process might be periodic, or at least have a characteristic frequency signature which could be used for vibration and fatigue analysis.

The modal analyzer was used to obtain power spectral density (Psd) data for each angle of attack from 0^{o} to 40^{o}. Integration of the Psd data over the frequency spectrum yields energy content of the fluctuating voltage across the hot film gage. The Psd integral is, in turn, a measure of the turbulent energy content of the airstream near the gage. Figure 2 is a graph of energy versus angle of attack. While these data show considerable scatter, the figure clearly indicates a trend of increasing energy content with angle of attack.

Figures 3 through 7 show the power spectra for the various angles of attack and speeds. Peaks in the Psd plots indicate frequencies which are characteristic of the flow. Thus a Psd graph which is relatively flat indicates a flow with no identifiable periodicity ("broad-band" turbulence). In contrast, a Psd graph with distinct peaks is indication of characteristic periodicity within the flow. For angles of attack of 0^{o} to 20^{o}, Psd's are very low-level over all frequencies, and without peaks to indicate a dominant frequency. Since all Psd plots from 0^{o} to 20^{o} appear the same,

only the 20° graph is shown (figure 3). For 25°, a distinct peak appears at V = 0.25 ft/sec, but is not visible for V = 0.58 and 0.75 ft/sec. For angles of attack of 30°, 35° and 40°, energy levels are distinctly higher, and dominant frequencies are discernable at all speeds tested.

To correlate model and full scale periodic phenomena or periodic phenomena for the same model at different speeds, a non-dimensional form of frequency is needed. This is provided by the Strouhal number, which is defined as follows:

$$\text{Strouhal number} = (f \times c)/V,$$

where: f = frequency, Hz

c = wing reference chord

V = free stream velocity.

Presumably, Strouhal number, like lift coefficient and other aerodynamic coefficients, will be relatively invariant with speed and scale. To test for consistency of Strouhal number, runs were made with tunnel speeds of approximately two and three times the nominal value. Dominant frequencies selected from the Psd graphs are plotted as frequency versus velocity for each angle of attack from 20° to 40° in figures 3 through 6. These results, taken from two separate test series, show that dominant frequency tends to increase linearly with tunnel velocity, indicating that Strouhal number is indeed constant with velocity. Furthermore, the Strouhal number is essentially a constant value of 0.7 for all angles of attack for which periodic behavior was observed.

CORRELATION WITH OTHER TESTS

The observation that Strouhal number is approximately constant with velocity is a crucial finding from these experiments. These results lend validity to the use of small scale tests, since they show that Strouhal number is independent of Reynolds number, at least for the test range of velocities. Furthermore, wind tunnel tests of a 12% scale basic F/A-18 configuration at Reynolds numbers of 0.4 and 0.8 x 10^6 by McDonnell-Aircraft Company (ref. 3) have shown nearly the same location for LEX vortices, nearly the same angle of attack for vortex bursting, and nearly the same Strouhal number for unsteady fin surface pressures. These correlations are strong evidence that the fundamental flow patterns are independent of Reynolds number, even for the very low Reynolds numbers of the water tunnel tests. Achieving this correlation for the basic model gives credibility to conclusions from water tunnel test results with the non-standard configurations. The merit of water tunnel experiments is the ability to quickly and inexpensively evaluate trends and essential features of flows associated with a wide variety of configurations. More detailed tests in wind tunnels and flight with a narrower range of configurations are still essential to validate final design configurations.

CONCLUSIONS

1. Surface hot-film anemometry shows high turbulent activity on the fins at conditions coincident with vortex bursting observed from flow visualization.
2. LEX vortex bursting occurs directly forward of the fin leading-edge for angles of attack of 25° and higher.
3. The onset of vortex bursting produces flow unsteadiness with a dominant frequency at a Strouhal number of 0.7 for three speeds and for angles of attack from 25° to 40°.
4. LEX vortex bursting is associated with wing separation and stalling. Removing the wing produced substantial changes in vortex positions and delayed vortex bursting.
5. Vortex bursting is unaffected by the fins. Removal of the fins had no appreciable effect on vortex locations or vortex bursting.
6. Vortex frequencies, vortex bursting, and dominant frequencies from the water tunnel tests correlate well with wind tunnel tests at higher Reynolds numbers.

REFERENCES

1. Erickson, G.E.: "Water Tunnel Flow Visualization and Wind Tunnel Data Analysis of the F/A-18," NASA CR-165859, May 1982.

2. Wentz, W. H. and Kohlman, D. L.: "Vortex Breakdown on Slender Sharp-Edged Wings," AIAA Journal of Aircraft, vol.8, no.3, pp. 165-161, March 1971.

3. McDonnell Aircraft Personnel: "F/A-18 Fin Buffet," Project briefings on fin buffet at Naval Air Development Center (NADC), 21 May 1986.

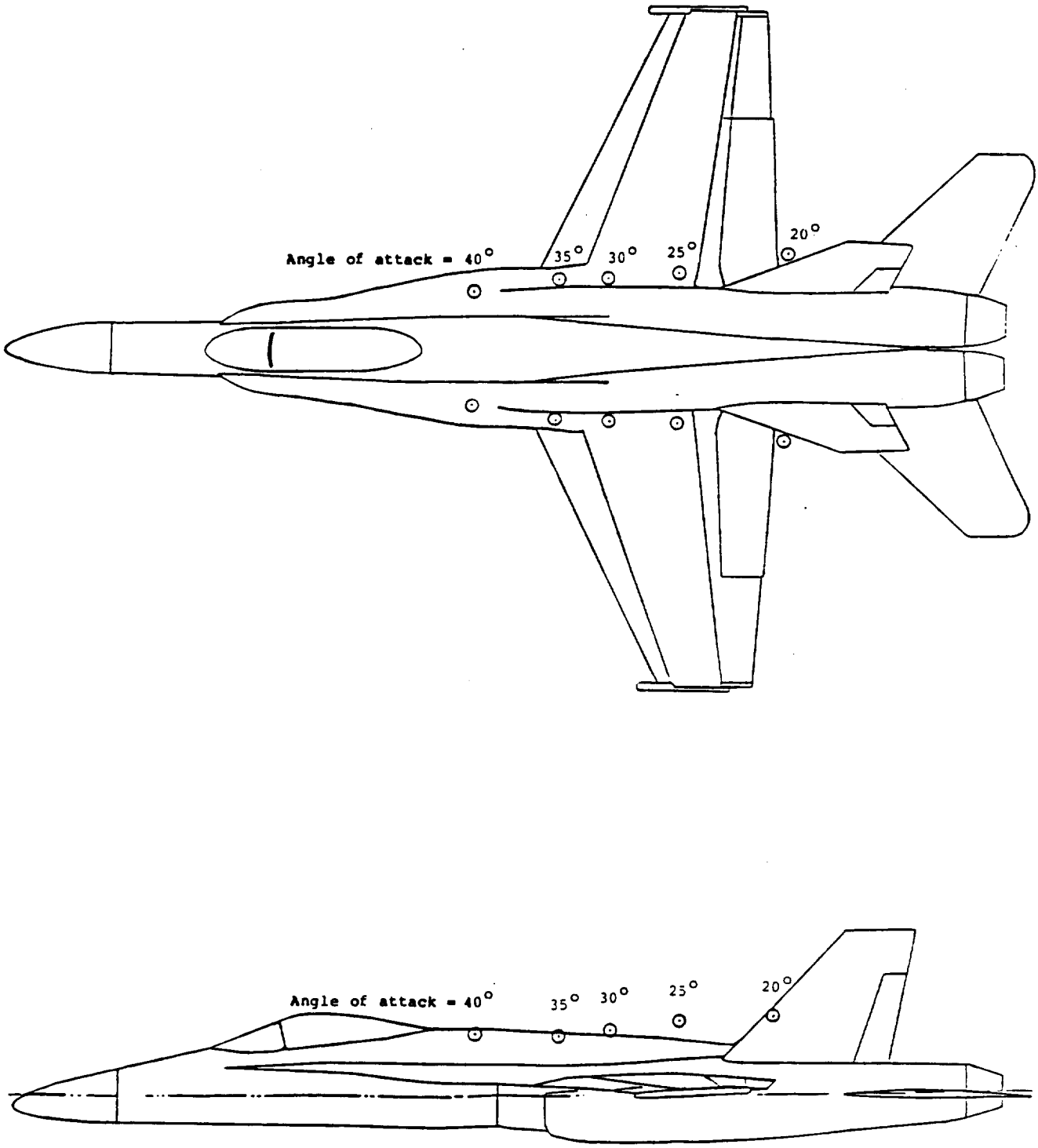

(a) Basic Model

Figure 1. Configurations and Vortex Burst Locations

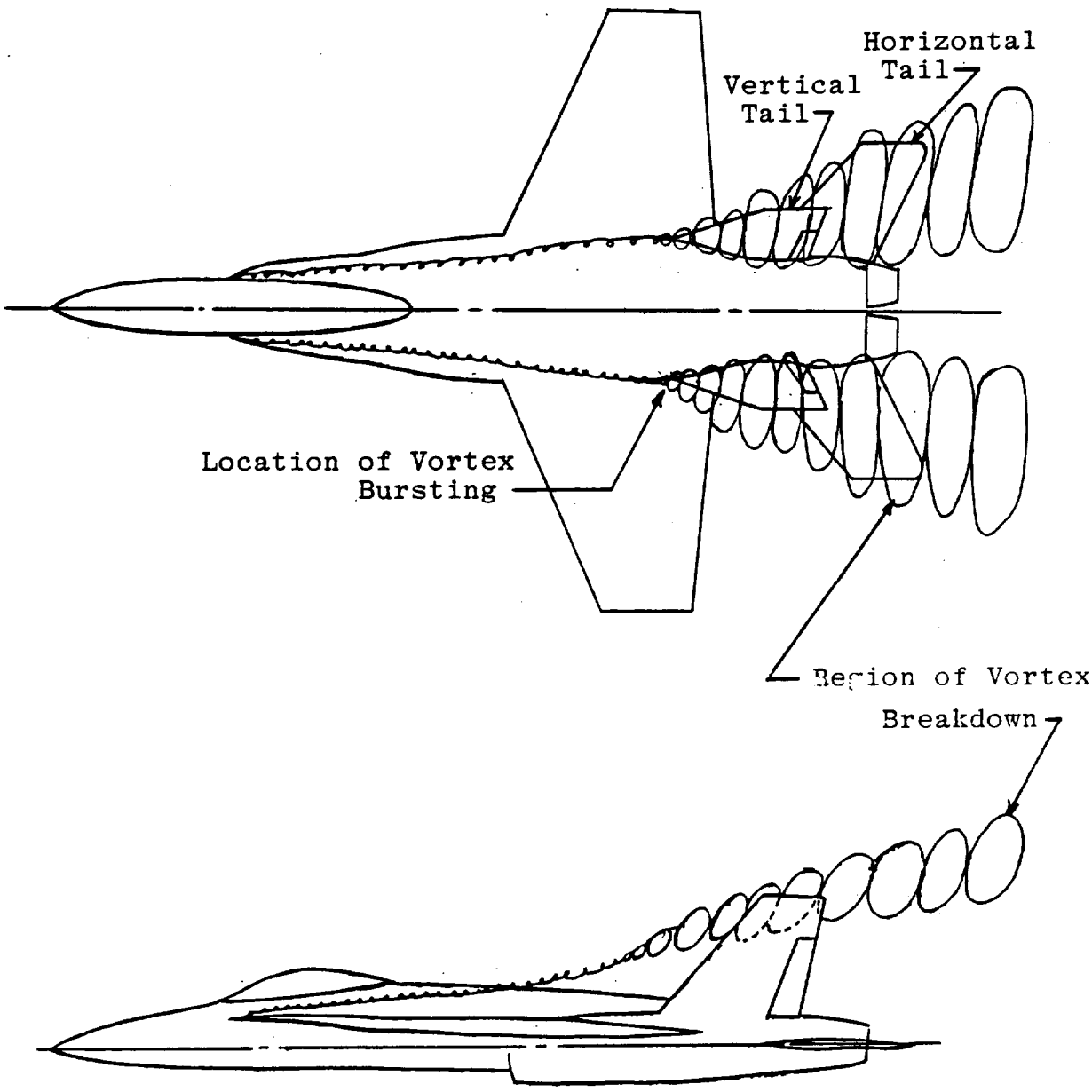

(b) Sketches of Vortex Flow Field After Bursting at an Angle of Attack of 25 Degrees

Figure 1. Continued.

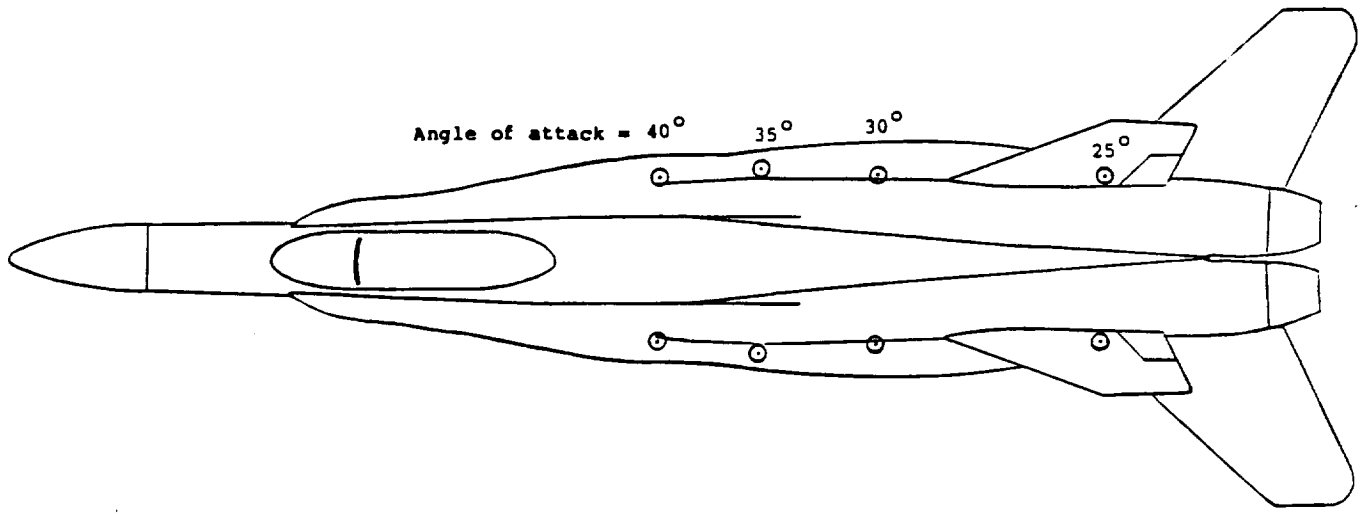

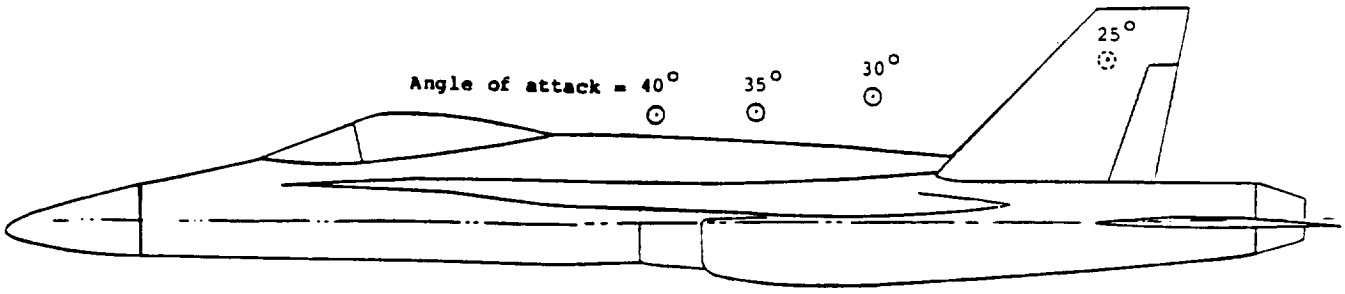

(c) Model Without Wings

Figure 1. Continued.

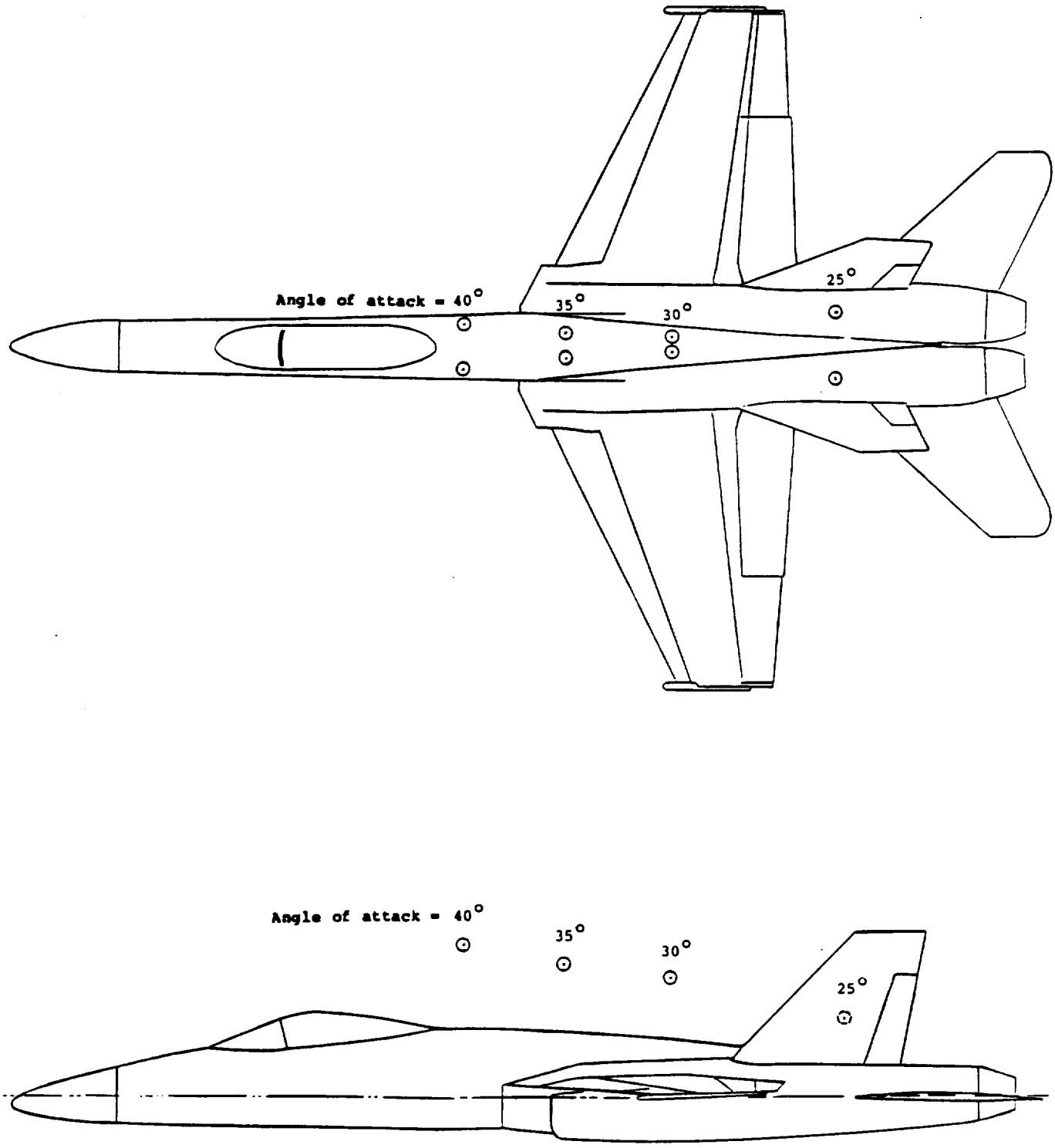

(d) Model Without LEX's

Figure 1. Concluded.

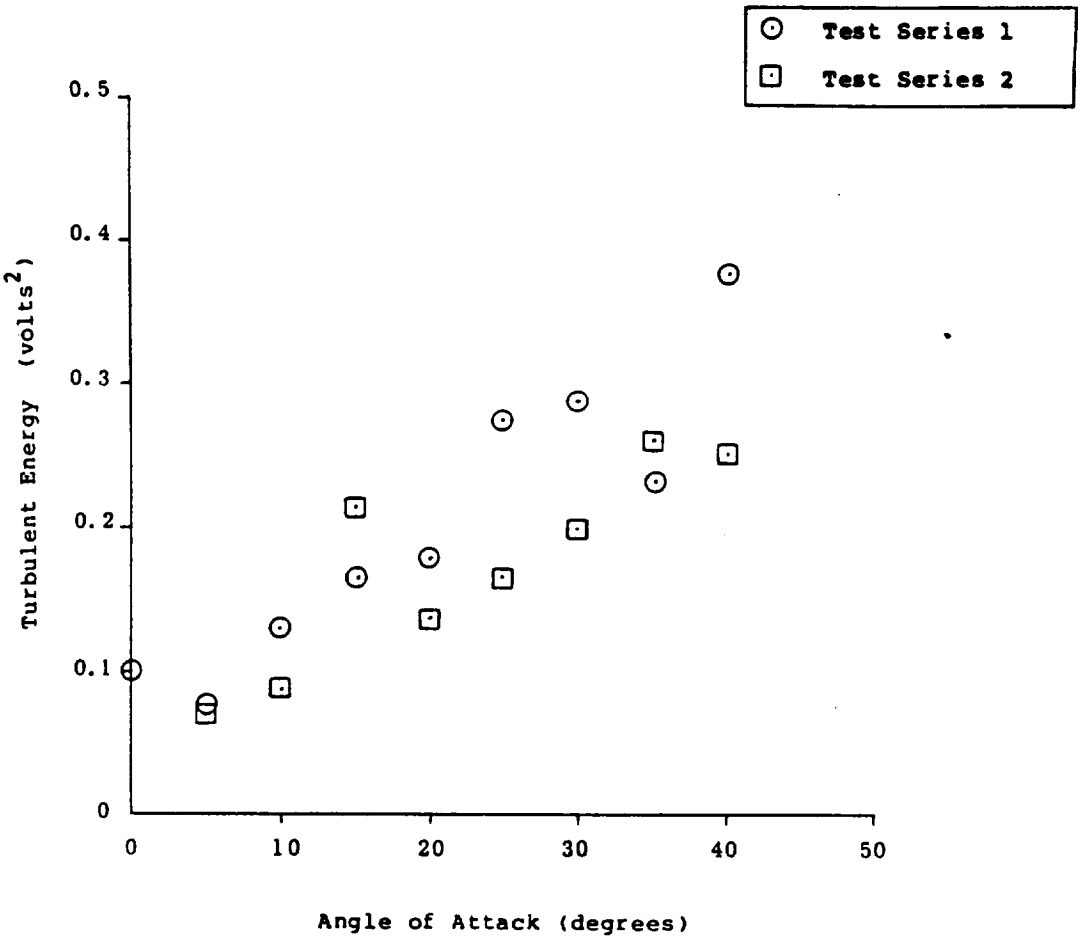

Figure 2. Turbulent Energy at Fin, V = 0.25 ft/sec

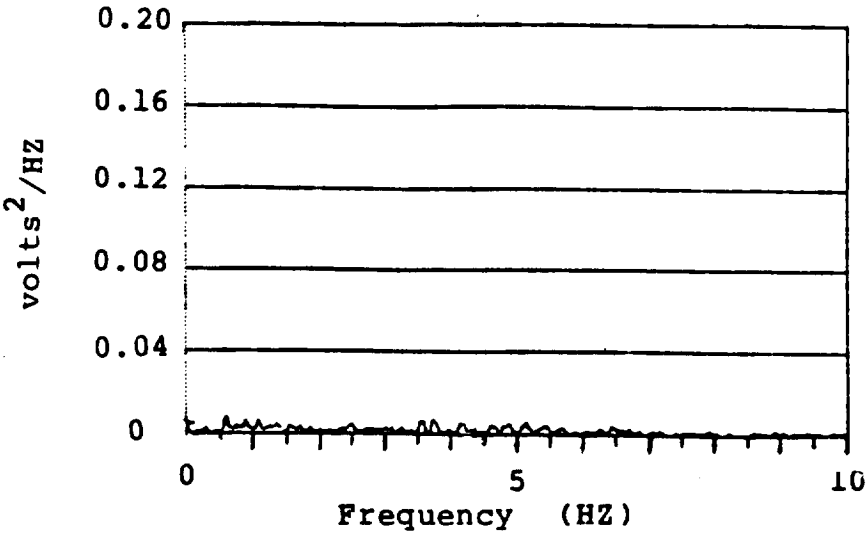

Figure 3. Power Spectral Density, Alpha = 20°, V = 0.25 ft/sec

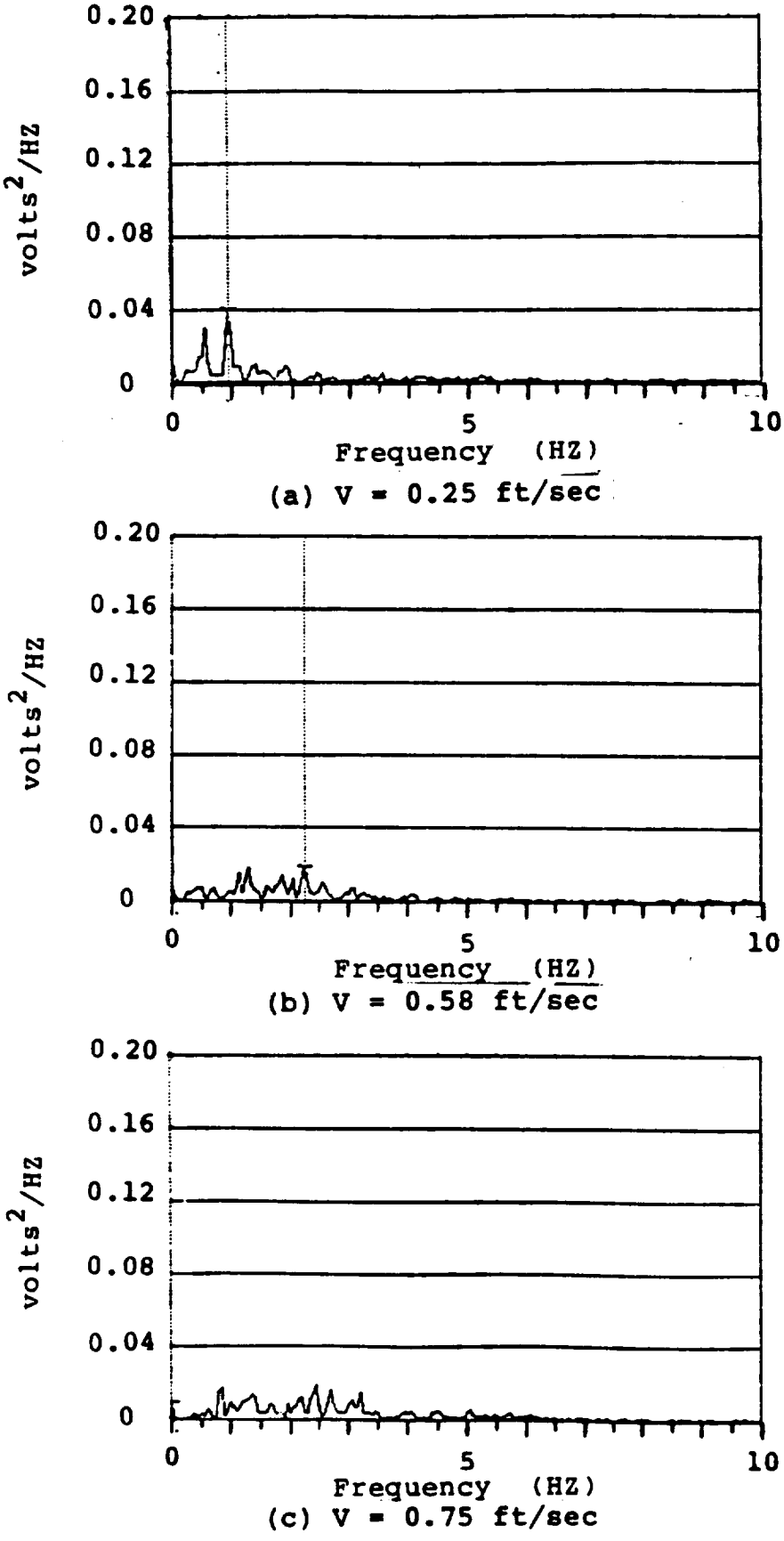

Figure 4. Power Spectral Densities, Alpha = 25°

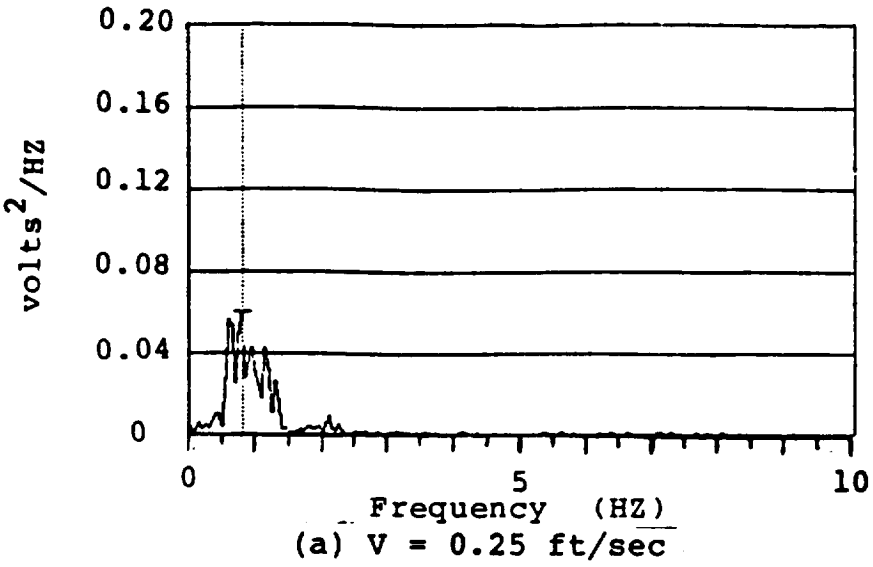

(a) V = 0.25 ft/sec

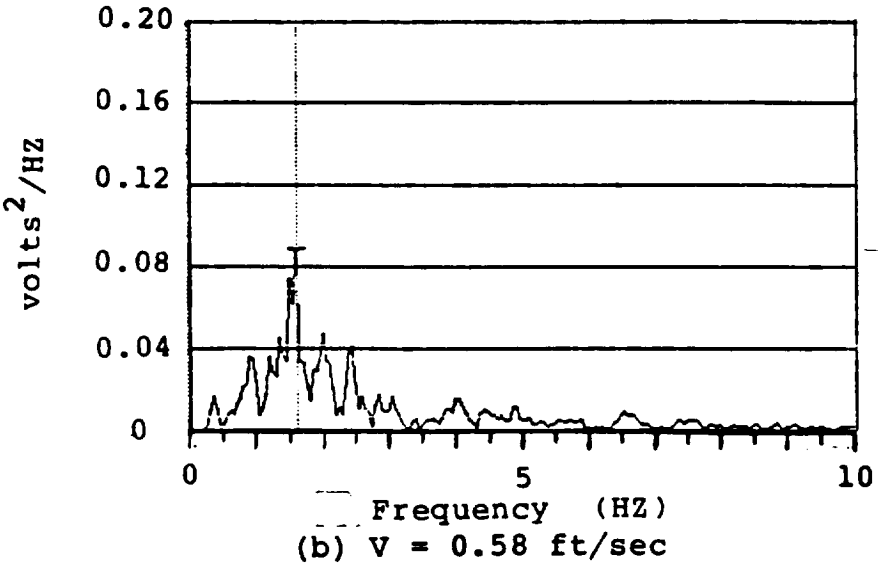

(b) V = 0.58 ft/sec

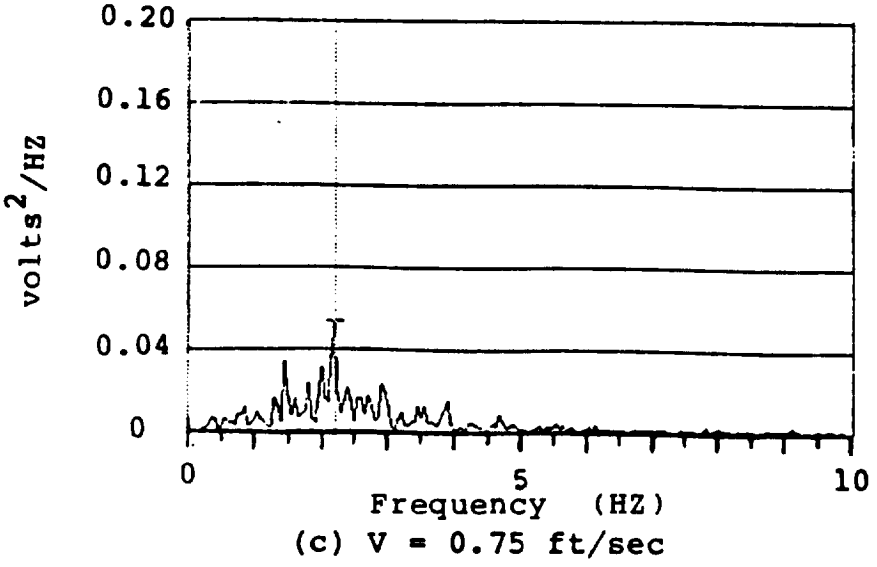

(c) V = 0.75 ft/sec

Figure 5. Power Spectral Densities, Alpha = 30°

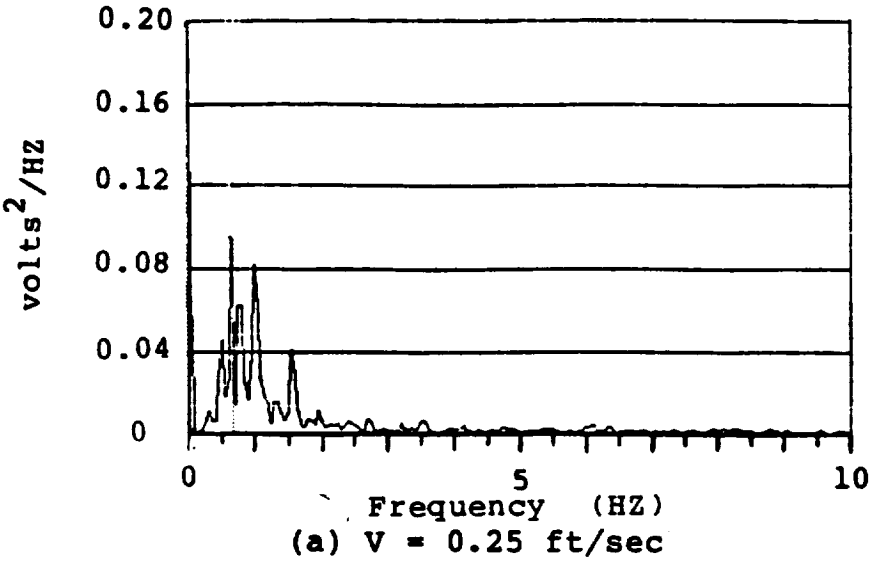

(a) V = 0.25 ft/sec

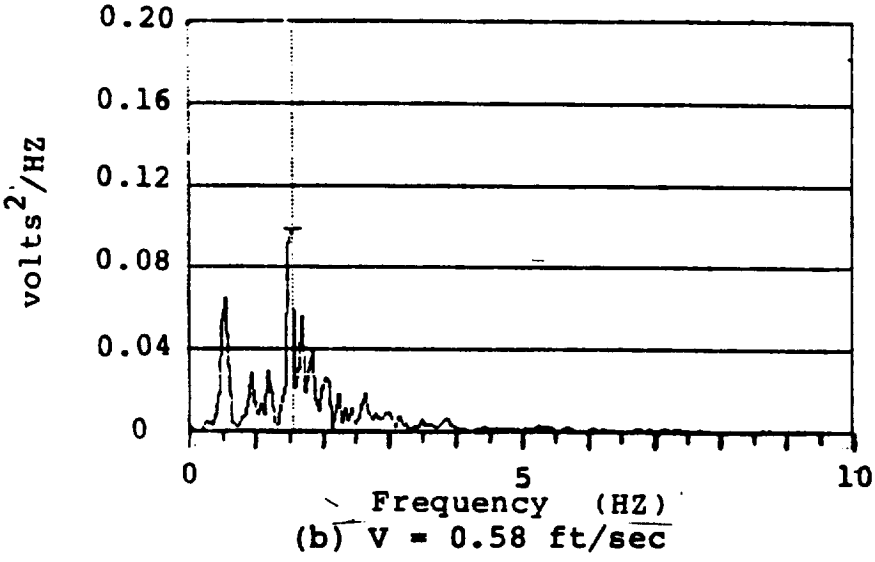

(b) V = 0.58 ft/sec

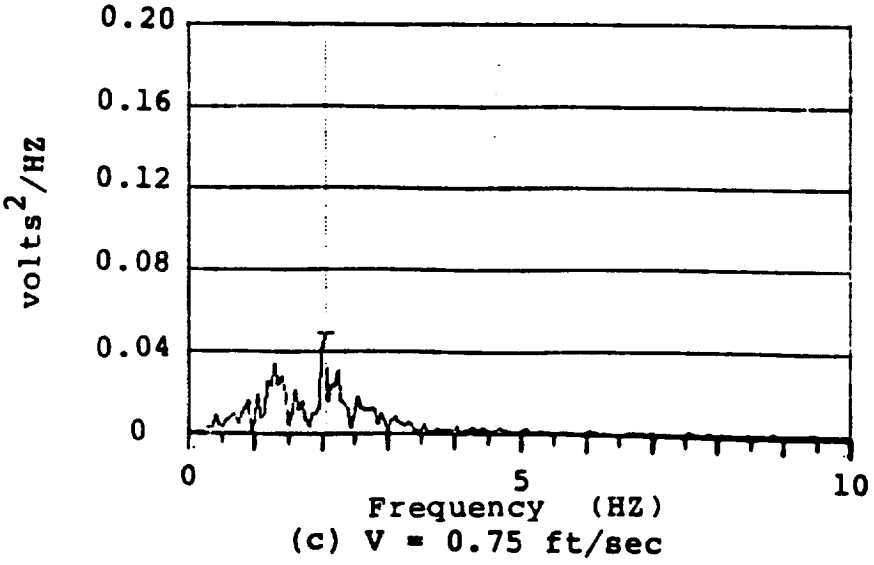

(c) V = 0.75 ft/sec

Figure 6. Power Spectral Densities, Alpha = 35°

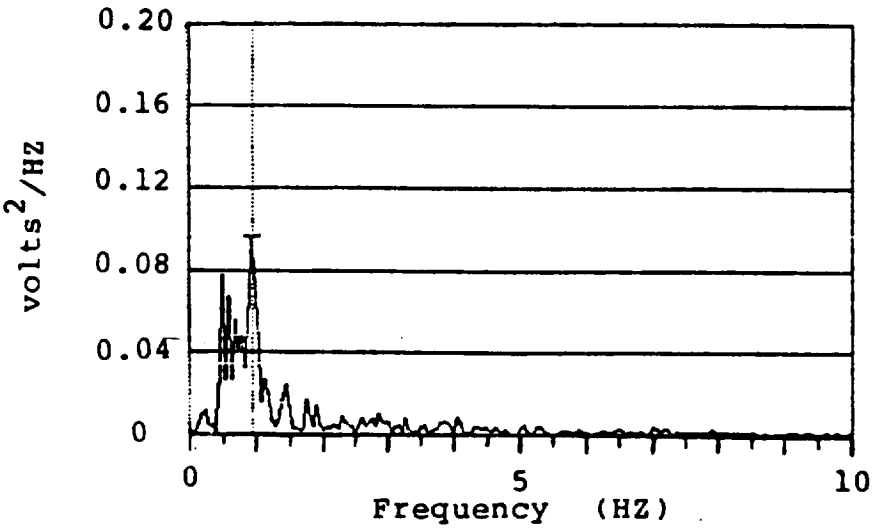

Figure 7. Power Spectral Density, Alpha = 40°, V = 0.25 ft/sec

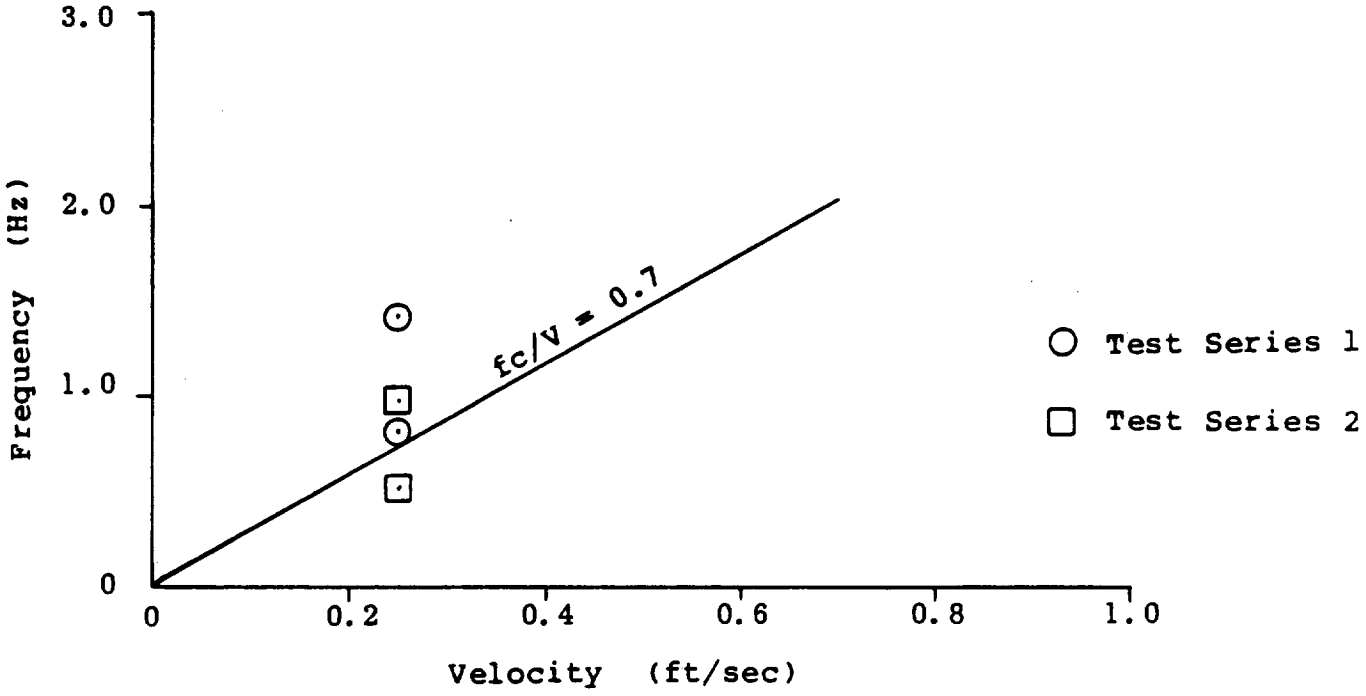

(a) Alpha = 25°

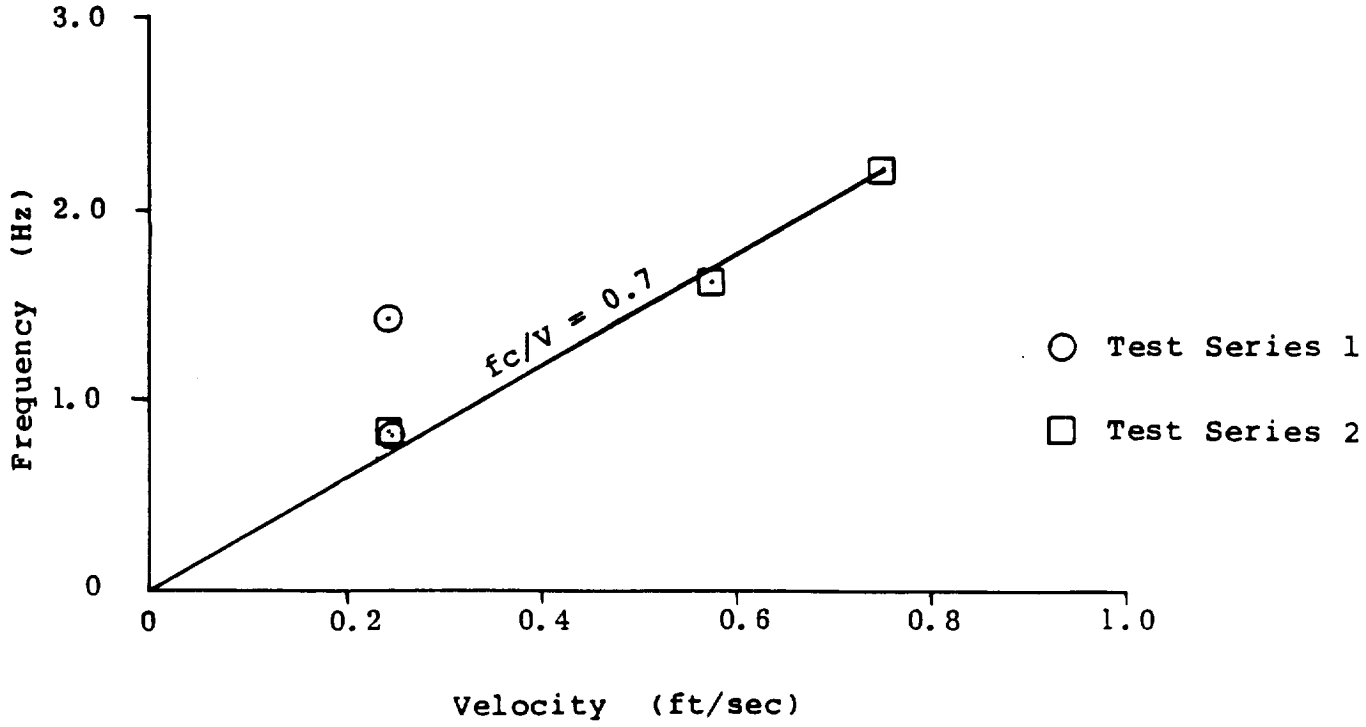

(b) Alpha = 30°

Figure 8. Dominant Frequency and Strouhal Number

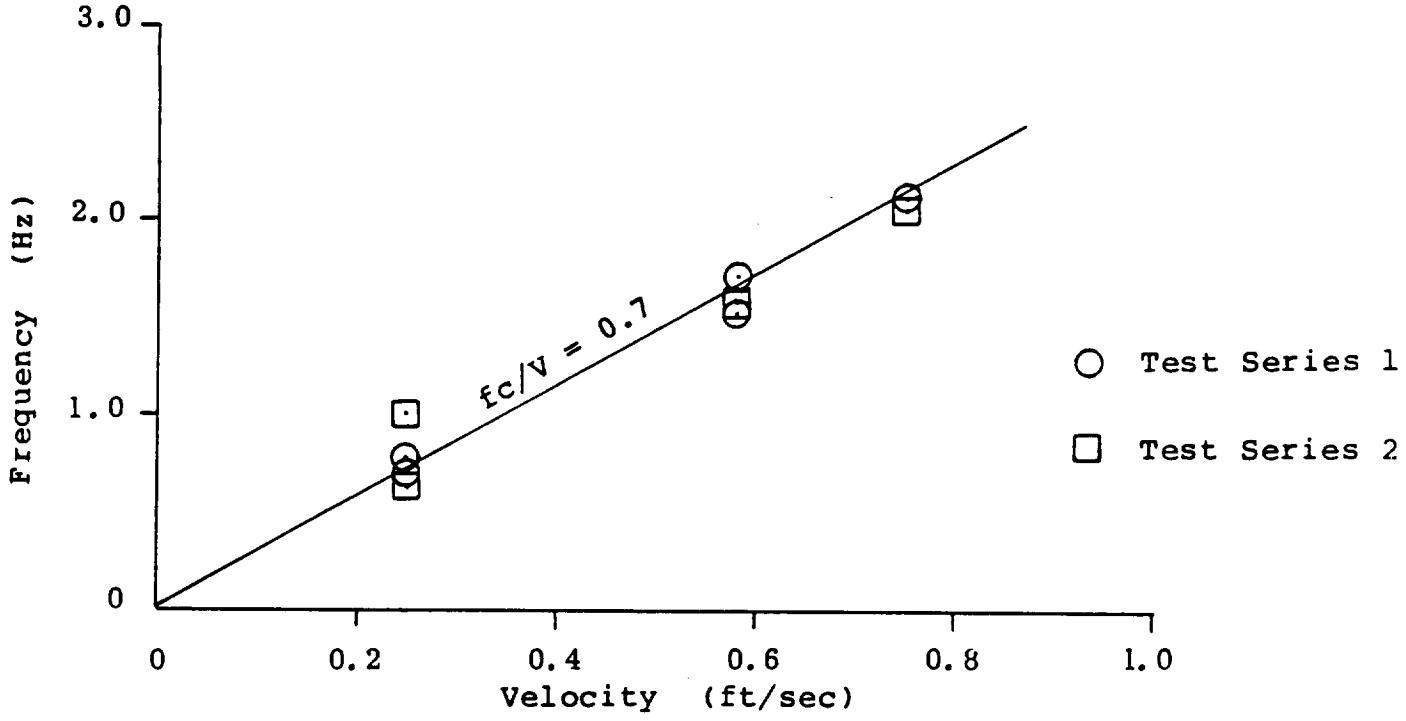

(c) Alpha = 35°

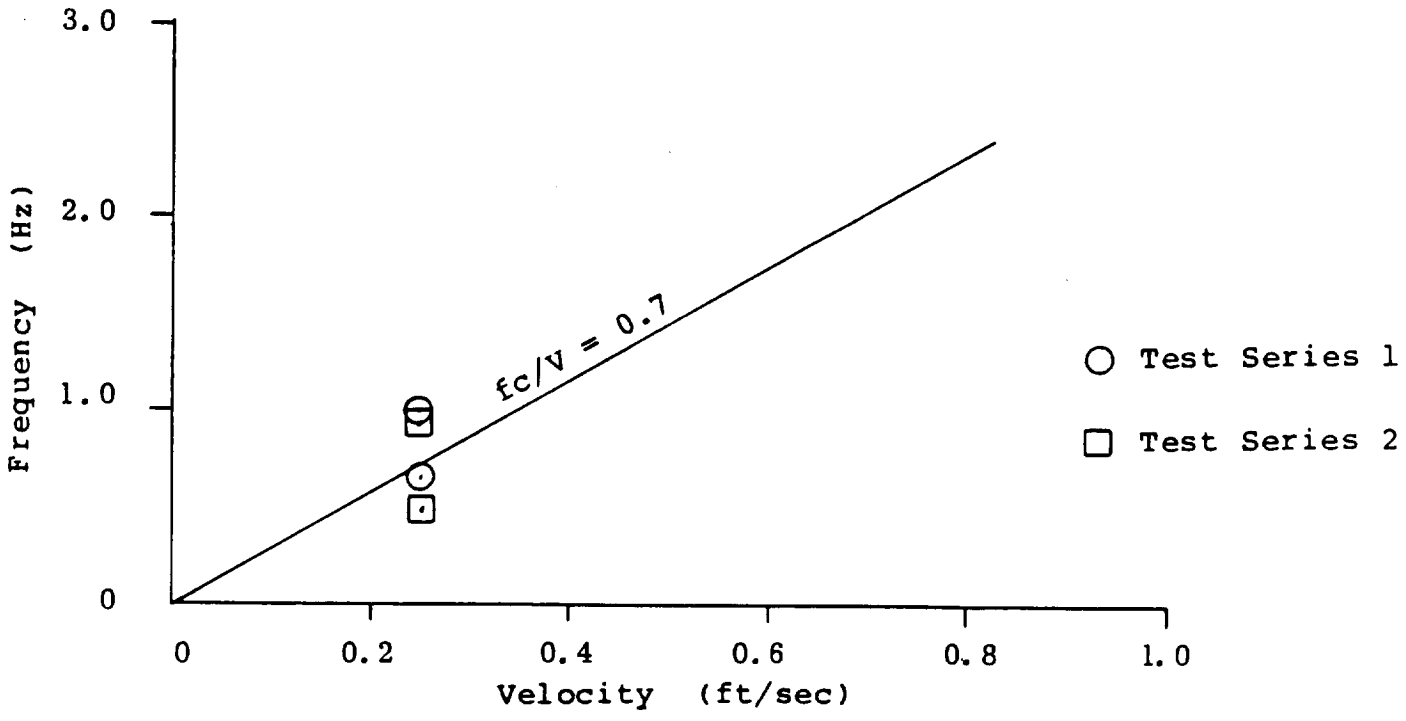

(d) Alpha = 40°

Figure 8. Concluded.

1. Report No.	2. Government Accession No.	3. Recipient's Catalog No.
NASA CR-179426		

4. Title and Subtitle	5. Report Date
Investigation of Empennage Buffeting	March 1987
	6. Performing Organization Code

7. Author(s)	8. Performing Organization Report No.
C. Edward Lan and I.G. Lee	H-1393
	10. Work Unit No.
	RTOP 505-68-71

9. Performing Organization Name and Address	11. Contract or Grant No.
Flight Research Laboratory University of Kansas Center for Research, Inc. Lawrence, Kansas 66045	NAG2-371
	13. Type of Report and Period Covered
	Contractor Report-Final

12. Sponsoring Agency Name and Address	14. Sponsoring Agency Code
National Aeronautics and Space Administration Washington, DC 20546	

15. Supplementary Notes

NASA Technical Monitor: David F. Fisher, Ames Research Center, Dryden Flight Research Facility, Edwards, California 93523-5000. NADC Technical Monitor: Ed Deska, Code 6041, Naval Air Development Center, Warminister, PA 18974-5000.

16. Abstract

Theoretical methods of predicting aircraft buffeting are reviewed. For the buffeting due to leading-edge vortex breakdown, a method is developed to convert test data of mean square values of fluctuating normal force to buffeting vortex strength through an unsteady lifting-surface theory and unsteady suction analogy. The resulting buffeting vortex from the leading-edge extension of an F-18 configuration is used to generate a fluctuating flow field which produces unsteady pressure distribution on the vertical tails. The root mean square values of root bending moment on the vertical tails are calculated for a rigid configuration.

Results from a flow visualization and hot film study in a water tunnel facility using a 1/48 scale model of an F-18 are included in an appendix by Dr. William H. Wentz, Jr. of Wichita State University. The results confirm that the LEX vortex is the dominant forcing function of fin buffet at high angles of attack.

17. Key Words (Suggested by Author(s))	18. Distribution Statement
Buffeting Vortex breakdown Vortex flow Water tunnel	Unclassified — Unlimited Subject category 39

19. Security Classif. (of this report)	20. Security Classif. (of this page)	21. No. of Pages	22. Price*
Unclassified	Unclassified	83	A05

For sale by the National Technical Information Service, Springfield, Virginia 22161.